Interfaces and Interphases in Ca and Mg Batteries

ADVANCED MATERIALS INTERFACES
www.advmatinterfaces.de

Interfaces and Interphases in Ca and Mg Batteries

*Juan D. Forero-Saboya, Deyana S. Tchitchekova, Patrik Johansson, M. Rosa Palacín, and Alexandre Ponrouch**

The development of high energy density battery technologies based on divalent metals as the negative electrode is very appealing. Ca and Mg are especially interesting choices due to their combination of low standard reduction potential and natural abundance. One particular problem stalling the technological development of these batteries is the low efficiency of plating/stripping at the negative electrode, which relates to several factors that have not yet been looked at systematically; the nature/concentration of the electrolyte, which determines the mass transport of electro-active species (cation complexes) toward the electrode; the possible presence of passivation layers, which may hinder ionic transport and hence limit electrodeposition; and the mechanisms behind the charge transfer leading to nucleation/growth of the metal. Different electrolytes are investigated for Mg and Ca, with the presence/absence of chlorides in the formulation playing a crucial role in the cation desolvation. From a R&D point-of-view, proper characterization alongside modeling is crucial to understand the phenomena determining the mechanisms of the plating/stripping processes. The state-of-the-art is here presented together with a short perspective on the influence of the cation solvation also on the positive electrode and finally an attempt to define guidelines for future research in the field.

1. Introduction

The increasing relevance of energy storage within current and future socioeconomic scenarios has prompted intensive research efforts aiming to unravel new technologies and concepts. The overarching aims are advantages in terms of performance, cost, and environmental impact with respect to the state-of-the-art. For the specific case of batteries, alternatives to lithium-ion batteries (LIB) are sought, which should hold promise of high energy densities while at the same time being based on abundant materials. One route is based on the use of divalent metals, such as calcium, Ca, or magnesium, Mg, as negative electrodes.[1] Both elements are very abundant, fifth and eighth, respectively, in the Earth's crust, resulting in low raw materials cost as compared to the lithium counterparts. Additionally, their metal foils exhibit electrochemical capacities much higher than those of the graphite-based negative electrodes used in LIBs.

Proof-of-concept for rechargeable Mg batteries was provided already in 2000,[2] but its technological development has been hampered by both the limitations of electrolytes enabling Mg plating/stripping and the development of suitable positive electrode materials. The analogous Ca concept has been investigated to a much lesser extent; recent efforts have unraveled suitable electrolyte formulations as well as promising estimates of prospective figures of merit at the cell level,[3,4] but breakthroughs are still needed.

While significant efforts have been made to enhance the technology readiness level (TRL) for both concepts, especially targeting positive electrode materials and electrolytes, the mechanisms of metal plating and stripping at the negative metal electrodes have attracted less attention.[5,6] Because electrochemical reactions take place at the electrode/electrolyte interfaces, the engineering of these is crucial to enable successful mass and charge transport. Note that reactivity at the interface may result in the formation of an interphase with a certain thickness, consisting of insoluble products which can act as passivation layer preventing further reaction. Depending on its composition/homogeneity, this interphase may or may not enable ionic and electronic transport, and hence it will be crucial in the efficiency of redox reactions. Throughout this text the various electrode/electrolyte interfaces will be denoted "interphases," with this broader term being preferred to indicate possible heterogeneity in composition and thickness, and the focus is on the nature of the negative electrode/electrolyte interphases and their impact on the plating/stripping processes.

First, we address the fundamental knowledge gained on cation solvation in the bulk of the electrolyte, a phenomenon and property which is an essential pre-requisite for a

J. D. Forero-Saboya, D. S. Tchitchekova, M. R. Palacín, A. Ponrouch
Institut de Ciència de Materials de Barcelona
ICMAB-CSIC
Campus UAB, Bellaterra, Catalonia 08193, Spain
E-mail: aponrouch@icmab.es
P. Johansson
Department of Physics
Chalmers University of Technology
Gothenburg 41296, Sweden
P. Johansson
ALISTORE-European Research Institute
CNRS FR 3104, Hub de l'Energie, Rue Baudelocque, Amiens 80039, France
The ORCID identification number(s) for the author(s) of this article can be found under https://doi.org/10.1002/admi.202101578.

DOI: 10.1002/admi.202101578

proper understanding of desolvation at electrolyte/electrode interphases. The crucial differences existing between Mg and Ca overall are herein highlighted, the concepts involving the latter relying on more standard battery electrolyte formulations, much alike those successfully used for LIBs. For Mg the differences between chloride-containing electrolytes, initial enablers of successful Mg plating, and more recently developed less corrosive concepts, are the paths followed. Second, we discuss the presence/absence of interphases acting as passivation layers on the surfaces of the electrodes—a more or less direct consequence of the electrolyte composition. Their composition and homogeneity are addressed, both affecting ion transport as well as nucleation and growth of metallic deposits, including dendrite formation in some cases. All along an effort is made to discuss experimental findings in conjunction to modeling studies, as the latter are extremely useful to rationalize the former.

The scarce current knowledge on the positive electrode/electrolyte interphases is briefly mentioned followed by a global discussion of the current state of the art and the potential paths to follow to increase the TRL for Mg and Ca batteries.

2. Mg^{2+} and Ca^{2+} Cation Solvation

As for all metal electrodes, the Mg and Ca plating/stripping coulombic efficiency and associated kinetics are strongly dependent on the nature of the electrolyte and the electro-active species: the cation complexes. Here, we briefly review the Mg and Ca electrolyte families developed during the past decades, the cation complexes they form, and the effect of their structure and dynamics on the properties at/of the interphases.

2.1. Chloride-Containing Mg Electrolytes

Historically, research on the solvation of magnesium cations in organic electrolytes started with magnesium organo-aluminate complexes formed in tetrahydrofuran (THF) solutions of R_xMgCl_{2-x} and R'_yAlCl_{3-y} (R = Et, Me), commonly known as dichloro-complex (DCC) electrolytes.[7] By the time, these were the only electrolytes from which reversible Mg plating/stripping could be achieved. Briefly, ligand exchange takes place between the Mg and Al metallic centers forming different cationic and anionic complexes: $MgCl_2$, $MgCl^+$, $Mg_2Cl_3^+$, R_4Al^-, $[R_2ClAl\text{-}Cl\text{-}AlClR_2]^-$, etc., with the exact proportion being dependent on the R groups and the Mg:Al:R:Cl ratios.[8,9] A combination of chloride and THF ligands are always found in the Mg first solvation shell, and a coordination number (CN) of six was commonly assumed. Much later the Mg^{2+} solvation in DCC electrolytes was investigated by density functional theory (DFT) calculations in gas phase[10] and showed that the complex formation energy exceeds 2 eV for neutral species such as $MgCl_2$ and Mg_2Cl_4, and can even be doubled or tripled for positively charged species, e.g., $MgCl^+$ and $Mg_2Cl_3^+$, suggesting that desolvation of Mg^{2+} from the latter at the electrolyte/electrode interphase may be penalized energetically. However, to draw realistic conclusions on Mg desolvation impact on the plating efficiency, both the effect of full solvation (beyond the first solvation shell) and interactions with the Mg metal electrode need to be accounted for. From first principles molecular dynamics (MD) simulations a strict preference for tetrahedral Mg coordination (CN = 4) in the monomers was deduced, but for the dimers also fivefold coordination (CN = 5) can be observed, with a minor difference in the formation energy, down to 35 meV, i.e., on the order of kT at room temperature (≈25 meV). These CN were verified by comparing the calculated Mg K-edge X-ray absorption spectra (XAS) spectra[10] with experimental data.[11]

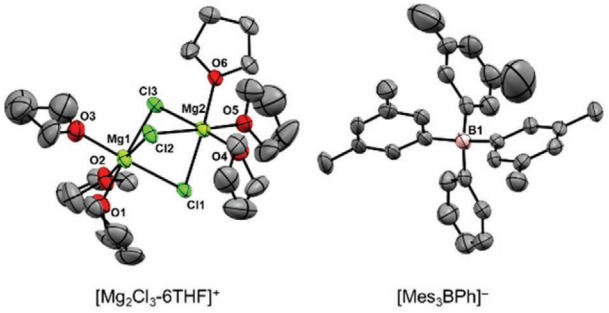

Figure 1. Molecular structures of complexes of the crystallized Mes_3B-$(PhMgCl)_2$ APC electrolyte. Adapted with permission.[15] Copyright 2012, The Royal Society of Chemistry.

Moving from the DCC electrolytes, Pour et al. replaced the alkyl group in R_xMgCl_{2-x} by a phenyl ligand, demonstrating an improvement in anodic stability for the resulting $(PhMgCl + AlCl_3)$/THF formulation, known as the all phenyl complex (APC) electrolyte.[12] In this electrolyte, the presence of $[Mg_2(\mu\text{-}Cl)_3 \cdot 6THF]^+$, $MgCl_2 \cdot 4THF$, and $[Ph_yAlCl_{4-y}]^-$ (y = 0-4) complexes was proven by combining Raman and multinuclear NMR spectroscopies with single-crystal X-ray diffraction (XRD).

When a nonpolar co-solvent is slowly added to a magnesium organohaluminate solution, a crystalline solid is obtained in which $Mg_2(\mu\text{-}Cl)_3^+$ dimer is the only cationic species.[13] The same cation was observed in other chloride-containing magnesium electrolytes using either Al- or B-based anions (**Figure 1**)[14,15] and its presence in solution has also been suggested from Raman spectroscopy data.[12]

Further improvement in the anodic stability of Mg electrolytes was achieved with the development of the magnesium aluminum chloro complex (MACC) electrolyte, $MgCl_2$+$AlCl_3$, containing only inorganic salts, which also enables reversible Mg deposition.[16] The speciation of the MACC electrolytes has been extensively studied experimentally and a variety of Mg—Cl complexes found, with the ratio between them being dependent on the $MgCl_2$:$AlCl_3$ ratio as well as the solvent and concentration.[17,18]

For THF as solvent, the cationic monomer $[MgCl(THF)_3]^+$ and the dimer $[Mg_2(\mu\text{-}Cl)_3(THF)_6]^+$ complexes, together with the $AlCl_4^-$ anionic complex, have all been detected in solution by Raman and ^{27}Al NMR spectroscopies.[19,20] In tetraglyme (G4) based MACCs with 1:2 or 1:3 $MgCl_2$:$AlCl_3$ ratios, presence of $AlCl^{2+}$, as observed by ^{27}Al NMR spectroscopy, results in Mg corrosion, Al codeposition, and low Mg plating/stripping coulombic efficiency (**Figure 2**).[21]

Regardless of the solvent used, the first plating/stripping cycles using a MACC electrolyte show low coulombic efficiency and high overpotentials, with the reaction kinetics remarkably

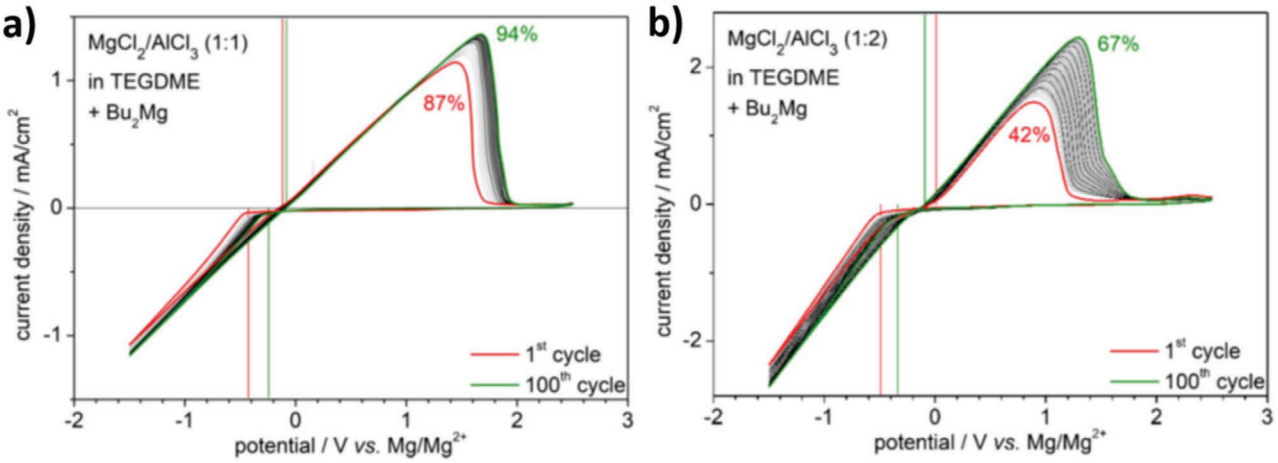

Figure 2. Cyclic voltammograms of a Pt WE in Bu_2Mg (10×10^{-3} M)-containing a) $MgCl_2/AlCl_3$ (1:1), b) $MgCl_2/AlCl_3$ (1:2), based on the 0.2 M Mg-salt in G4, from 1st to 100th cycle, $\nu = 25$ mV s^{-1}. Reproduced with permission.[21] Copyright 2019, American Chemical Society.

improving after several cycles. During this "conditioning" process, some Al deposits are formed, effectively modifying the Mg:Al ratio and their speciation in solution.[17,21]

The overall properties of THF based MACC electrolytes have been investigated also by both DFT calculations and classical MD simulations and, surprisingly, only a few types of species were found likely/present, with double charged species appearing to be unstable in this electrolyte.[22] By DFT the formation energies of various hypothetical Mg—Cl complexes were calculated as function of the CN of the Mg^{2+} cation. These indicated the most stable complexes to be $[MgCl(THF)_3]^+$ and $MgCl_2(THF)_2$ (both CN = 4), the dimer $[Mg_2Cl_3(THF)_4]^+$ (CN = 5), and the trimer $[Mg_3Cl_5(THF)_6]^+$ (CN = 6). Their existence was further confirmed by the Mg-O(THF) radial distribution functions (RDFs) obtained from the MD simulations, overall highlighting that the typical sixfold coordination of Mg^{2+} in solids is not always observed in solution. The effect of the MACC electrolyte composition on the stability of the complexes was studied by analyzing the Mg-Cl-Al-THF chemical space. Results indicate that for the Mg-Cl-THF sub-system at the bulk THF chemical potential, only $[MgCl(THF)_3]^+$ and $MgCl_2(THF)_2$ are stable species with neither the dimer $[Mg_2Cl_3(THF)_4]^+$ nor the trimer $[Mg_3Cl_5(THF)_6]^+$ being stable, in agreement with the formation of monomeric species at the interphase during Mg deposition.[23] At lower THF chemical potential, the dimer $[Mg_2Cl_3(THF)_4]^+$ is only ≈+0.02 eV above the ground state line, hence the authors hypothesize that it may form under solvent evaporation/drying, explaining why it was successfully isolated from crystalized APC electrolyte.[12] The corresponding Al-Cl-THF subsystem renders $[AlCl(THF)_2]^{2+}$, $[AlCl_2(THF)_2]^+$, $AlCl_3(THF)$, and $AlCl_4^-$ as stable species. The 4D Mg-Al-Cl-charge phase diagram indicates only plausible equilibria, respecting charge neutrality, between either $[MgCl(THF)_3]^+$ with $AlCl_4^-$, or the neutral $MgCl_2(THF)_2$ with $AlCl_3(THF)$. A detailed overview on the MACC electrolyte speciation can be found in a recently published review.[24]

However, despite the high efficiency of the Mg electrodeposition process in the above chloride-containing electrolytes, these electrolytes are highly corrosive, significantly limit the anodic stability, and are commonly associated with the use of highly volatile solvents (such as THF or DME) which hampers any practical application. Replacing Cl^- by other anions has been the subject of recent research efforts, but alternative electrolyte formulations have not come easy (Section 2.2). Finally, in contrast to the many Mg conducting electrolytes, there have been no similar efforts on Grignard type electrolytes made for Ca.

2.2. Chloride-Free Electrolytes for Ca and Mg Batteries

2.2.1. Electrolytes with Borohydrides and Other Boron-Containing Anions

Metal borohydrides are primarily known for their application as hydrogen storage materials and as strong reducing agents.[25] The simple BH_4^- anion presents a high stability against electrochemical reduction, its calcium and magnesium salts are soluble in some organic solvents, and being a reducing agent it can act as a water scavenger. Its low stability against electrochemical oxidation, however, limits its application coupled to high voltage positive electrode materials.

Studying $Mg(BH_4)_2$ in THF based electrolytes, Hahn et al. observed the formation of neutral species, ion pairs, and higher aggregates, to be dominant for the concentration range 0.1–1.1 M, and this to put a severe limit on the tractable ion conductivity: <0.03 mS cm^{-1}.[26] Replacing THF by a chelating solvent such as dimethoxyethane (DME, also denoted as monoglyme or G1) can improve the salt dissociation and increase the ratio of both monocharged ion pairs $[Mg(BH_4)]^+$ and free BH_4^- anions, as proven by ^{25}Mg and ^{11}B NMR spectroscopy.[27] A more general study of $Mg(BH_4)_2$ based electrolytes was made via MD simulations, by analyzing the local solvation in seven different solvents: dimethylamine (DMA), acetonitrile (ACN), dimethyl sulfoxide (DMSO), THF, G1, diglyme (G2), and tetraglyme (G4).[28] Overall, at 0.4 M concentration, THF as well as the chelating solvents with a connecting N atom (ACN and DMA) were found to exhibit poor Mg^{2+} solvation, with aggregates being observed. For the glymes, the salt dissociation

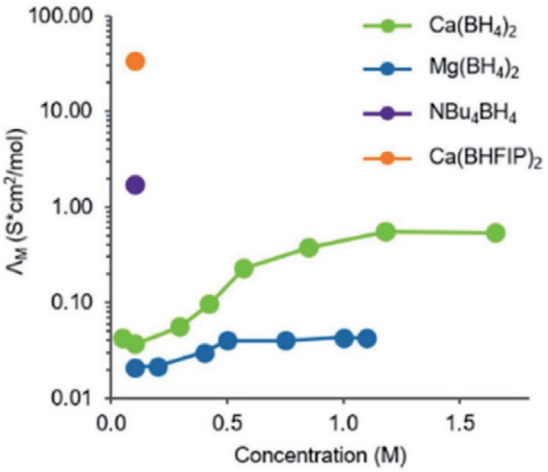

Figure 3. Molar ionic conductivities for some selected salts in THF as a function of concentration (BHFIP = tetrakis(hexafluoroisopropyloxy)borate). Reproduced with permission.[30] Copyright 2020, The Royal Society of Chemistry.

improves as a function of chain length, i.e., from G1 to G4, yet the best solvent was found to be DMSO. In the two latter solvents, G4 and DMSO, only contact ion pairs (CIPs) were found to be formed and no aggregates.

For the Ca analogue, Ta and co-workers suggested the cation–anion interactions in $Ca(BH_4)_2$ in THF electrolytes not to be very strong and the Ca^{2+} cation to be entirely surrounded by solvent molecules even at 1 M concentration.[29] This is in stark contrast to the dielectric relaxation spectroscopy studies from Hahn et al., that suggested formation of neutral aggregates as well as $[Ca(BH_4)]^+$ and $[Ca(BH_4)_3]^-$.[26] Even though significantly higher ionic conductivity was found for the Ca case as compared to the analogous Mg electrolyte (**Figure 3**), it is still very low (0.0038 mS cm^{-1} at 0.1 M) compared to a less associating tetrabutylammonium (NBu_4^+) based electrolyte (0.17 mS cm^{-1}). This implies undissociated neutral species to be present/dominant also for Ca.

To the best of our knowledge, neither the $Ca(BH_4)_2$ solubility nor the solvation structure in other solvents than THF has been experimentally investigated, even though other solvents may improve the ionicity and hence the ion conductivity (*ionicity* is understood as the fraction of total ions available to conduct charge according to the definition by MacFarlane et al.[31]). Using a combination of DFT and COSMO-RS modeling approaches, however, these properties (amongst others) were screened for $Ca(BH_4)_2$, and three other Ca salts, for no less than 81 solvents.[32] This showed that BH_4^- anions tend to bind Ca^{2+} cations very strongly and that the dissociation energy of the formed ion pairs is higher than when other anions are used.

Another borohydride anion example, the monocarborane cage-style anion $[CB_{11}H_{12}]^-$ has historically been proposed as an extremely weakly coordinating anion (WCA).[33] However, both the Ca and Mg salt solubilities are in general low.[34] Only the G3 and G4 solvents enabled $Mg(CB_{11}H_{12})_2$ solubility to any reasonable extent, but it can be enhanced by using solvent mixtures such as THF/G1, 1,3-dioxolane (DOL)/G1, DOL/G2, THF/G2, or G1/G2 (**Figure 4**). The Mg^{2+} first solvation shell in G1/G2 was found to involve both solvents, forming $[Mg(G2)(G1)_2]^{2+}$ complexes with a hypothesized CN = 7, based on ^1H NMR spectroscopy studies.[35]

Similarly to the Mg case, the $Ca(CB_{11}H_{12})_2$ salt shows very limited solubility in G1 and THF, but dissolves readily in G1/THF mixtures producing electrolytes with high ionic conductivities, up to 4.0 mS cm^{-1}.[36] The Ca^{2+} first solvation shell has not been determined, but likely both solvents participate, as for Mg^{2+}.

In contrast to the above mentioned case, both the Mg and Ca salts of the $[B(hfip)_4]^-$ (tetrakis(hexafluoroisopropyloxy)borate) anion were found to be readily dissociated in single solvent THF and G1 electrolytes.[37] For Ca^{2+} in THF, a CN = 6 was reported, while higher CNs were found for G1, G2, and G3. The solvation structure for $Mg[B(hfip)_4]_2$ has not been completely characterized, but a higher tendency for ion pairing is expected given the higher charge density of Mg^{2+} cation.

A recent study reported a higher ionic conductivity for $Mg[Al(hfip)_4]_2$ electrolytes in glymes, compared to equivalent systems using the alkoxyborate $[B(hfip)_4]^-$ anion, indicating that the former exhibit better ion dissociation and/or higher charge carrier mobilities. The formation of anion–solvent complexes and hence the decrease of anion mobility and increase in t_+, suggested by MD simulations, is presented as the origin for

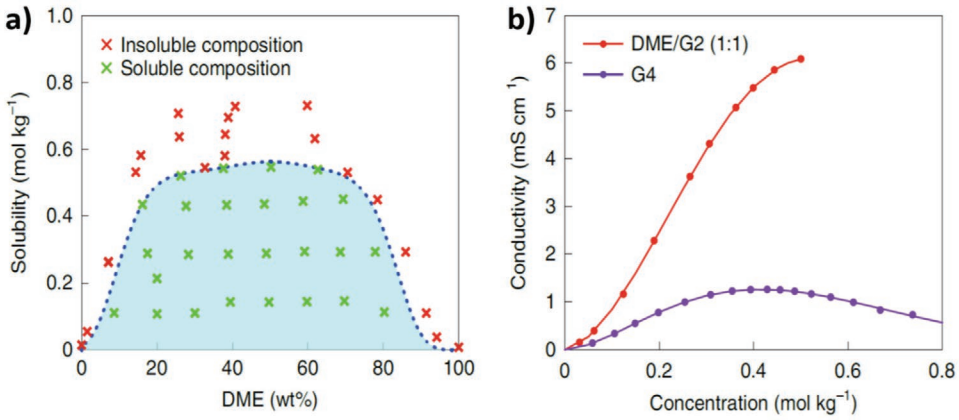

Figure 4. a) Solubility of $Mg(CB_{11}H_{12})_2$ in G1/G2. b) Ionic conductivity as function of $Mg(CB_{11}H_{12})_2$ concentration in G4 and G1/G2 at 25 °C. Reproduced with permission.[35] Copyright 2020, Springer Nature.

the improved ionic conductivity.[38] However, we believe this to be unlikely, as previous reports in lithium-ion electrolytes have shown that anion trapping results in a decrease of the overall ionic conductivity of the electrolyte.[39]

Finally, the solvation of $Ca(BF_4)_2$ in organic carbonate solvents, both single and equimolar mixtures, was found to be highly solvent-dependent.[40] MD simulations indicate a cation CN = 8 to be preferred for ethylene carbonate (EC), propylene carbonate (PC), and vinylene carbonate (VC), and one BF_4^- anion also participating in the cation first solvation shell. For butylene carbonate (BC) and dimethyl carbonate (DMC), a CN = 6 dominates, with two BF_4^- anions completing the first solvation shell. In equimolar mixtures, EC/PC, EC/EMC, EC/DMC, total CN = 9 are observed. DFT calculations show the Ca^{2+} cations to primarily be coordinated by the solvent carbonyl oxygen atoms and to a lesser extent by the BF_4^-, while only weak interactions were detected with the solvent etheric ring oxygen atoms. Alternative DFT calculations of optimized $[Ca(BF_4)_n]^{2-n}$ structures determined CN = 3, 6, 6, and 7, respectively for n = 1, 2, 3, and 4, confirming possible mono-, bi-, and tridentate coordination modes for the BF_4^- anion.[32]

Overall, one of the main challenges for Ca and Mg conducting electrolytes based on boron-containing anions is to achieve a significant degree of salt dissociation, to avoid the formation of CIPs and aggregates. The most promising strategies employed thus far to that end have been based on: chelating solvents, such as glymes, WCAs, such as $[B(hfip)_4]^-$, and/or solvent mixtures, where each solvent can have a different impact on the energetics and kinetics of cation desolvation.

2.2.2. Electrolyte Formulations Containing TFSI

As a WCA, from its highly delocalized charge, the bis(trifluoromethanesulfonyl)imide (TFSI) anion represents an interesting alternative also for Mg and Ca based electrolytes as before for both Li and Na analogues.[41]

Indeed, no CIPs were detected in $Mg(TFSI)_2$ electrolytes using G4,[42] G3,[43] G2,[44] G1,[45] or ACN[46] as solvents. Significant Mg^{2+}-TFSI interactions are observed when solvents with lower dielectric constants, such as 2-MeTHF, are used.[46] But not only the dielectric constant is responsible for an effective cation-anion separation in solution, both the chelating nature and the donor number (DN) (or Lewis basicity) of the solvent also play important roles. This can be evidenced when using high dielectric constant carbonate solvents, such as EC or PC, for which some degree of ion pairing is obtained, even at low salt concentrations of 0.1 M, possibly due to their lower DNs as compared to glymes.[47]

Further insight on the Mg^{2+} coordination by the glyme family of solvents in the presence of TFSI anions was provided by the combined experimental-computational work on $Mg(TFSI)_2$ in G2 and G3 electrolytes.[43,48] Using Raman spectroscopy and DFT calculations in conjunction,[43] it was demonstrated that the Mg^{2+} ions are solvated by two G3 molecules forming $[Mg(G3)_2]^{2+}$ complexes, where each G3 acts in three modes: bidentate, tridentate, and tetradentate, forming multiple complexes such as $[Mg(tri\text{-}G3)_2]^{2+}$ and $[Mg(bi\text{-}G3)(tetra\text{-}G3)]^{2+}$, the former being the preferred one. In G2 electrolytes, at $Mg(TFSI)_2$ concentrations ≤0.92 M,[48] octahedral $[Mg(G2)_2]^{2+}$ complexes were detected by IR spectroscopy. DFT calculations point to a tridentate coordination only, i.e., CN = 6, was determined in such complexes. The difference between the G2 and G3 based electrolytes might be related to entropy rather than enthalpy, as only one complex, $[Mg(tri\text{-}G2)_2]^{2+}$, exists in the former.[48] Based on this, the authors suggest that the room temperature solubility of $Mg(TFSI)_2$ in G3 (<≈1.6 M), appreciably larger than in G2 (<≈1 M), may be ascribed to the larger variety of Mg^{2+}–G3 complexes formed.

Interactions between Mg^{2+} and TFSI were suggested by proper quantitative analysis of RDFs from MD simulations,[28] but also interactions with solvents such as G1, G2, G4, DMSO, and THF, and differently with N chelating solvents (ACN and DMA). Formation of aggregates was suggested for ACN, DMA, G1, and THF, the latter two presenting weak Mg–O interactions, the same trend was observed for $Mg(BH_4)_2$, described above. The Mg^{2+} cations have CN = 6 by DMSO and G4, hence no CIPs but solvent-separated ion pairs (SSIPs), meanwhile the CN = 6 for the G2 electrolyte is completed by G2 and one or more TFSI oxygen atoms, hence CIPs. As for the aggregates formed, the protic nature of DMA provides a better anion coordination and thereby a larger solubility of this electrolyte. Indeed, the solvent coordination for TFSI is higher for DMA than for ACN, G1, and THF, which shows that even though DMA has a very low dielectric constant it can promote a better dissociation of $Mg(TFSI)_2$. These results on the glyme solvents contrast with previous DFT calculations, finding only well solvated Mg^{2+} complexes with G2 and G3 and no interaction with the TFSI anion.

Later, 0.1–1.2 M $Mg(TFSI)_2$ in G1 electrolytes were investigated by MD simulations,[49] showing no CIPs but Mg^{2+} solely coordinated by ≈3 G1 (CN = 6), in agreement with Raman and NMR spectroscopy results.[45] This is thus in contrast to the conclusions drawn in ref. [28], which perhaps is due to the earlier work using a nonpolarizable force field for the classical MD simulations, while the more recent work applied a polarizable one. The main impact of the inclusion of polarizability is a better reproduction of the real G1 conformer population and thereby the local structure of the Mg^{2+} first solvation shell, with the polarizable force-field simulations favoring a denser G1 solvent "packing", thus excluding the TFSI anion, in better agreement with the experimental data.

Spectroscopic results suggest that $Ca(TFSI)_2$ is more readily dissociated than the corresponding Mg salt, due to the lower polarizing power of the Ca^{2+} cation as compared to Mg^{2+}.[47] $Ca(TFSI)_2$ was found to be completely dissociated at concentrations ~ 0.1 M, with an average of six solvent molecules surrounding each cation, while CIPs start to emerge when the concentration is increased above ≈0.5 M in most solvents. Notably, the solvation number (SN) in dimethylformamide (DMF) did not change up to 1.2 M $Ca(TFSI)_2$ concentration, suggesting that both ion pair and aggregate formation in this electrolyte are negligible. This finding was also confirmed by a combined DFT COSMO-RS study[32] wherein after a large screening of solvents, DMF was preferably used as a high DN solvent. $[Ca(DMF)_8]^{2+}$ (CN = 8) was found to be the energetically preferred complex, as compared to CIPs and higher aggregates, especially for the PF_6^- and TFSI based salts. Overall,

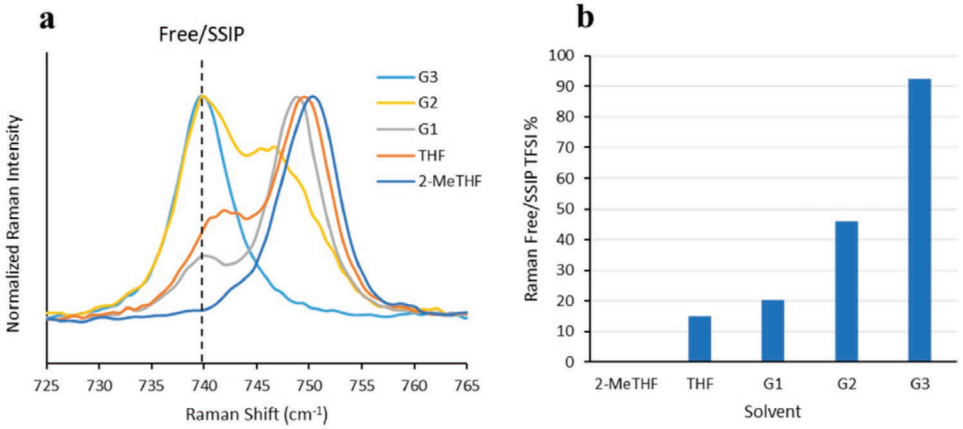

Figure 5. a) Raman spectral comparison of the TFSI breathing mode region for solutions of ≈0.5 M $CaTFSI_2$ in various ether solvents. The frequency of the free/SSIP TFSI mode is indicated by a dashed line. b) Calculated percentage of the integrated Raman signal intensity corresponding to the free/SSIP TFSI mode in each solvent. No free/SSIP TFSI was observed in 2-MeTHF. Reproduced with permission.[50] Copyright 2020, American Chemical Society.

these comparative results fundamentally point to $Ca(TFSI)_2$ and $Ca(PF_6)_2$ in DMF electrolytes to be promising from a physicochemical point-of-view, but so far no plating/stripping has been achieved.

The tendency to form Ca^{2+}-anion CIPs in ether and glyme based electrolytes was investigated by Hahn et al. using a similar Raman spectroscopy approach.[50] They concluded that the probability of CIPs increases as: G3 < G2 < G1 < THF < 2-MeTHF (**Figure 5**), again pointing to the cation chelating ability to be an important factor—as these solvents have little variation in their dielectric constants. Furthermore, using metadynamics sampling, the authors determine the relative coordination tendencies of TFSI and G1, G2, and G3 toward Ca^{2+}. The number of minima is largest for G1, four with similar free energies and also includes a CIP configuration (consistent with the Raman data), while for both G2 and G3, there are only two local minima for each, both fully solvating the cation much stronger than for G1 as solvent, and no CIPs present. Finally, by ab initio molecular dynamics (AIMD) simulations of $Ca(TFSI)_2$ in G1 and G3, the same authors infer a change from exclusively bidentate coordination for G3 to a mixed bidentate/monodentate coordination for G1—in this case the TFSI could also coordinate to the Ca^{2+} cation, and hence CIPs creation.

2.3. Electrolytes with Mixed Salts

Mixing different salts has been a common strategy to increase the ionic conductivity of divalent electrolytes, undoubtedly affecting the number but also the nature of the charge carriers in solution. Herein, the effect on the Mg^{2+} or Ca^{2+} first solvation shell will be discussed. Briefly, mixing anions (i.e., MX_2 + MY_2, M = Ca^{2+} or Mg^{2+}) may be used both to increase the cation concentration beyond the saturation value of a single salt electrolyte, and to alter the nature of the solvent shell by competition between X^- and Y^- anions, and this should possibly influence the desolvation kinetics at the metallic anode. In contrast, mixing cations (i.e., MX_2 + M′X, M = Ca^{2+} or Mg^{2+} and M′ = Li^+ or Na^+) increases the relative anion concentration versus the M^{2+} cations, and thereby promotes ion-pair formation.

Starting with the latter scheme, adding $LiBH_4$ increases the solubility of $Mg(BH_4)_2$ in ether solvents. At concentrations above 0.5 M in G4, $Mg(BH_4)_2$ is not completely soluble and forms cloudy electrolytes, but the addition of $LiBH_4$ to a final $[Li^+]$ = 1.5 M renders completely transparent solutions.[51] The increased solubility, together with the observed increased kinetics for plating/stripping, suggests a direct impact on the Mg^{2+} complexes.[52] It is also possible, however, that the improved performance is due to an increased total ionic conductivity or a more favorable Mg:Li alloy deposition (with up to 10 at% of Li, depending on the lower cut-off voltage during cyclic voltammetry [CV]), as suggested by Chang et al.[53]

Jie et al. studied $Ca(BH_4)_2$ and $LiBH_4$ in THF electrolytes[54] and found a similar effect; by ^{43}Ca NMR spectroscopy they showed a lower partial solvent CN for Ca^{2+}, suggesting that the anion is also coordinating when $LiBH_4$ is added. An evident improvement in the plating kinetics is observed, but the possibility of Li codeposition needs to be addressed in this kind of studies, particularly given that the Ca and Li reduction potentials are separated by less than 200 mV.

Wang et al. reported on a series of $Mg(TFSI)_2$ in G2 electrolytes, where few or no CIPs were detected for concentrations ≈0.4 M. When 0.1 M of $Mg(BH_4)_2$ was added, the anion displaces the TFSI in the cation first solvation shell, and thus the Mg^{2+}-TFSI ion pairs are broken and Mg^{2+}-BH_4^- ion pairs form.[55] A fast exchange between different solvation structures was established, suggested to enhance plating kinetics.[56] Yet, these conclusions are to be taken with due care as it has been suggested that the BH_4^- anion can also act as a water scavenger and improve plating kinetics simply by making the electrolyte drier.[57]

Chlorine ligands are also able to displace TFSI anions from the first solvation shell, as clearly shown by adding one equivalent of $MgCl_2$ to a $Mg(TFSI)_2(G3)_2$ solid adduct.[58] Several reports exist showing the efficiency of $MgCl_2$ as additive to improve plating/stripping from $Mg(TFSI)_2$ and $Mg(CF_3SO_3)_2$ in ether electrolytes (0.25 M $Mg(TFSI)_2$ + 0.5 M $MgCl_2$ in G1,[59] 0.2 M $Mg(CF_3SO_3)_2$ + 0.2 $MgCl_2$ in G1,[60] 0.5 M $Mg(TFSI)_2$ + various amounts of $MgCl_2$ in THF and G2[61]). However, the lack of systematization between these studies makes any

unambiguous comparison difficult. Nevertheless, the Cl^- ligands are expected to participate strongly in the solvation of the Mg^{2+} cation forming Mg—Cl complexes, as described in Section 2.1.

Aiming to understand the Cl^- contribution in these systems, the stability of the different species present in the $Mg(TFSI)_2$+$MgCl_2$ in G1 system against a Mg (0001) slab, as function of both the electrode potential and the Cl^- chemical potential, i.e., in direct relation to the Cl^- concentration, was investigated by building the corresponding Pourbaix diagram via DFT calculations.[62] When the Cl^- chemical potential, i.e., concentration increases, the initially predominant $[Mg(G1)_3]^{2+}$ was found to progressively convert into more chlorinated species: $[Mg_2Cl_2(G1)_4]^{2+}$, $[Mg_3Cl_4(G1)_5]^{2+}$, $[MgCl_2(G1)_2]^{2+}$, and $[MgCl_3(G1)]^-$. All species found in this model are consistent with experimental observations,[63] excepted the $[MgCl_3(G1)]^-$, as the high Cl^- chemical potential needed is not experimentally accessible, due to the low solubility of $MgCl_2$. The role of the chloride-containing species during Mg plating will be further discussed in Section 3.2.

3. Electrolyte Stability and Passivation Layer Formation

Understanding the interfaces between the negative electrode and the electrolyte, including the presence/absence of interphases, is critical to efficient battery performance and lifetime. In this section we review the stability of different electrolytes against the surfaces of Ca and Mg metal electrodes. We initially address the stability of the most common electrolyte solvents used and then progress to discuss the anions from the same perspective, using the same classification as sections above. For the cases where reactivity of electrolyte species versus the metal electrodes has been observed, a summary of the reported decomposition products is presented in **Tables 1** and **2**, respectively.

In addition to the possible decomposition products found in each electrolyte, Tables 1 and 2 also report the experimental conditions employed in each study, together with the analytic techniques employed. Traditionally, X-ray photoelectron (XPS), energy-dispersive X-ray (EDX), and IR spectroscopies have been the most used techniques, although electron energy loss (EELS) and XAS, and time-of-flight secondary ion mass spectrometry (TOF-SIMS) have gained attention recently. We acknowledge the importance of using complementary techniques to get deeper insight into the different decomposition products formed.

Various products observed on/at the Ca and Mg surfaces are analogous to those formed in LIBs for similar electrolyte formulations. However, we call for caution, as the insights gained after many years of LIB R&D indicate that the nature of such layers can be affected by impurities and be dynamic in nature evolving upon cycling, with conditions (including temperature) having a significant influence. Moreover, in some cases they can evolve during preparation for characterization, so their nature is tricky to elucidate. Along the same lines, even in electrolyte systems considered stable against Mg (or Ca) metal, small amounts of oxides and hydroxides can be found on the surface, but these are often attributed to contaminations from inside the glovebox rather than true electrolyte decomposition products[64] (see entries 1–4 in Table 1).

3.1. Stability of Solvents in Contact with Mg and Ca Surfaces

Early on, Aurbach et al. studied the stability of pure solvents and some few electrolytes in contact with Ca and Mg metals with the decomposition products being identified by IR spectroscopy.[65,66] Here, in contrast to LIB studies where a cation conducting solid electrolyte interphase (SEI) can be formed, when PC or ACN are used, insoluble decomposition products accumulate on the surface (possibly) blocking the transport of divalent cations, and thus further deposition. For PC, $Mg(OCO_2R)_2$ and $MgCO_3$ were unambiguously identified, and $CaCO_3$ and $Ca(OH)_2$ in Ca. ACN decomposition results in nonfully characterized condensation products in both Mg and Ca.

In contrast, ether solvents such as THF, G1, and other glymes were found to be stable, which made them solvents of choice for most subsequent studies of Mg plating and stripping. Glymes were only found to decompose when —OH groups are present at the Mg metal surface (as a result of water contamination of the electrolyte).[67] These results suggest that not only the electrolyte composition influences the formation of passivating surface films, but they impact, in turn, the future decomposition of the electrolyte.

Quantum mechanical modeling was used to study the changes induced in the electrochemical stability windows (ESWs) of ACN, THF, G1, and DMSO from interactions with either metallic Mg (unpassivated) or an insulating MgO-based surface, the latter being used as proxy mimicking a passivated Mg surface or an oxide-based positive electrode active material.[68] The LUMO and HOMO energy levels were demonstrated to be modified by the interfacial interactions with the surfaces, thus substantially reducing (up to 25%) the spread in solvent ESW at the interfaces, especially for solvents with large dipole moments, such as ACN and DMSO (**Figure 6**). This is in agreement with experimental studies of their reductive decomposition on Mg metal.[69] In contrast, the change is smaller for the modeling of interface versus MgO and/or solvents with smaller dipole moments, the latter being consistent with weaker electrostatic interactions with the surface. From this study we can conclude that ACN has the best anodic stability, but is the easiest to reduce, while DMSO is the easiest to oxidize and G1 presents the best cathodic stability. However, for a correct (quantitative) interpretation of the ESW, it is crucial to incorporate solvent–salt interactions (not included in the present model), which are known to impact the overall electrolyte stability.

By assuming various decomposition products, energetics of decomposed G1 configurations against three different electrodes—Mg (0001), MgO (100), and $MgCl_2$ (0001)—was studied by a combination of classical Monte Carlo coupled with vdW-DFT.[70] It was found that interaction of G1 decomposition products with Mg metal is highly exothermic, and may result in the evolution of ethylene gas, while being unfavorable on the latter two surfaces, where nearly zero reaction enthalpies and large reaction barriers were observed. However, these findings do

Table 1. Summary of decomposition products formed during electrochemical testing of several Mg electrolyte formulations reported in the literature.

Entry	Electrolyte	Conditions	Products observed at the surface	Techniques used	Refs.
1	Pure THF	Soak Mg electrodes in the solution	No decomposition of the solvent. Presence of MgO and $Mg(OH)_2$	XPS	[64]
2	Pure PC	Soak Mg electrodes in the solution	No evidence of PC reduction at the Mg surface. If so, a very thin layer would be forming	XPS	[64]
3	$PhMgCl + AlCl_3$ in THF (APC)	Galvanostatic deposition at 1 or 10 mA cm^{-2} over Cu electrodes	Mg-Cl aducts, Al codeposition	XPS, SEM, EDX	[121]
4		Cycling of Mg|Mg cell	No surface layer	XPS	[122]
5		Soak Mg electrodes in the solution	– No passivation layer on top of Mg when soaking it in the electrolyte. – $[Mg(THF)_5]^+$ accumulated at the surface	Operando XAS	[101]
6	$MgCl_2 + AlCl_3$ in THF (MACC)	Cyclic voltammetry over Pt electrodes	Al, Mg, Cl detected	SEM, EDX	[123]
7	$MgCl_2 + AlCl_3$ in G1 (MACC)	Galvanostatic deposition at 1 or 10 mA cm^{-2} over Cu electrodes	MgO, metallic Al, Al_2O_3, Mg—Al intermetallic deposit, CuO	XPS, SEM, EDX	[121]
8	$Mg(BH_4)_2$ in ether	Galvanostatic deposition at 10 mA cm^{-2} over Cu electrodes	Up to 10% B codeposition	–	[124]
9	$Mg(ClO_4)_2$ in PC	Soak Mg electrodes in the solution	$Mg(OCO_2R)_2$, magnesium halides, $Mg(OH)_2$, $MgCO_3$, ClO_4^- reduction products	FTIR, SEM, EDX	[66]
10	$Mg(TFSI)_2$ in G1	Cycling of Mg|Mg cell	F in the surface film. Anion decomposition	XPS	[122]
11	$Mg(TFSI)_2$ in G2	Stepwise polarization of a Mg electrode	$Mg(OH)_2$, MgO, MgF_2, diglyme decomposition products	Ambient pressure XPS	[67]
12		Galvanostatic deposition over GC electrodes	MgO, $Mg(OH)_2$ C, O, Cl at the surface N, S, F as either trapped anions or decomposition products	XPS	[105]
13		Cyclic voltammetry over Pt electrodes	TFSI decomposition products	XRD, XPS, XAS	[55]
14	$Mg(TFSI)_2$ in G3	Soak Mg electrodes in the solution	$Mg(OH)_2$, MgO, and MgX (X = halogen)	XPS	[125]
15	$Mg(TFSI)_2$ in G4	Soak Mg electrodes in the solution	More MgO, $MgCO_3$, and $Mg(OH)_2$ No evidence of MgF_2, $MgCl_2$, nor MgS	XPS, NEXAFS	[106]
16		Soak Mg electrodes in the solution	Significant amounts of O, F, and S → Clear evidence of decomposition of the $TFSI^-$	XRD, EDX, XPS	[91]
17		Galvanostatic deposition at 1 mA cm^{-2} for 12 h on a Cu electrode	MgF_2, MgS, other SOx compounds from anion decomposition	XRD, EDX, XPS	[91]
18	$Mg(TFSI)_2$ in ACN	Cycling of Mg|Mg cell	Solvent decomposition → ACN condensation products	XPS, FTIR	[122]
19		Soak Mg electrodes in the solution	Non identified ACN reduction/condensation products	FTIR, EQCM, EDX	[66]
20	$Mg[B(hfip)_4]_2$ in G1	Galvanostatic cycling over Cu surface	B—O, Mg—F, Mg—O moieties	EDX, XPS, TOF-SIMS	[86]
21		Soak Mg electrodes in the solution	No evidence of surface layer	EDX, XPS, TOF-SIMS	[86]
22	$Mg(CB_{11}H_{12})_2$ in G4	Cycling of Mg|Mg cell	No surface layer	XPS, SEM	[122]
		Soak Mg electrodes in the solution	MgO	XPS	[91]
23		Galvanostatic deposition at 1 mA cm^{-2} for 12 h on Cu electrodes	MgO	XPS	[91]
24	0.4 M $Mg(TFSI)_2$ + 0.1 M $Mg(BH_4)_2$ in G2	Cyclic voltammetry over Pt electrodes	No F, S, N, or B signals detected on the Mg deposit	XPS	[126]
25	0.25 M $Mg(TFSI)_2$ + 0.5 $MgCl_2$ in G1	Galvanostatic deposition at 1–5 mA cm^{-2} on Pt electrodes	Sulfur detected: TFSI decomposition products. When no $MgCl_2$ is added, the surface film appears more organic in nature	SEM, EDX, XPS	[59]

Table 1. Continued.

Entry	Electrolyte	Conditions	Products observed at the surface	Techniques used	Refs.
26	0.3 M $Mg(triflate)_2$ + 0.2 M $MgCl_2$ in G1	Cycling of Mg|Mg cell	MgO, $Mg(OH)_2$, MgF_2, $MgCl_2$ (and other Mg—Cl complexes), $MgCO_3$, MgS. The peaks corresponding to C and O organic species gets weaker in the deep layers. The inorganic compounds are more present.	XPS	[60]
27	$Mg(BH_4)_2$ + $LiBH_4$ in G1 or THF	Cyclic voltammetry over Pt electrodes	CIPs: $[Mg(\mu\text{-}H)_2BH_2]^+$ at the interface H_2(g) evolution B_xH_y clusters formed at the surface by anion decomposition	Operando Mg K-edge and B K-edge XAS operando TEM	[82]

not allow to infer on the adsorbed (intact) G1 molecule interaction with the corresponding surfaces, as possibility for charge transfer from the Mg surface to the adsorbed G1 molecule was not demonstrated. Based on previous study of G1 ESW versus Mg metal in ref. [68], where its LUMO level was found to be 600 mV above the Mg^{2+}/Mg level, adsorbed (intact) G1 is expected to be stable versus reduction on Mg surface. Nevertheless, results versus $MgCl_2$ surface may support the often-made notion/hypothesis that the presence of Mg–Cl interactions at or in the vicinity of the Mg surface can improve the electrochemical performance (Section 3.2).

The lower standard reduction potential of Ca metal promotes the decomposition of solvent molecules as compared to Mg metal. Both γ-butyrolactone (γBL) and PC decompose on contact with Ca metal producing cyclic β-ketoesters and $CaCO_3$, respectively, while ACN forms insoluble condensation products.[65]

A combined DFT and AIMD comparative study on the decomposition of pure EC solvent and a $Ca(ClO_4)_2$ in EC electrolyte at a Ca (001) metal surface indicates that $CaCO_3$, CaO, and $Ca(OH)_2$ should be primary inorganic interphase components.[71] For pure EC, even though a fast two-electron reduction producing carbonate (CO_3^{2-}) and ethylene (C_2H_4) is thermodynamically and kinetically favored, a reaction producing ethylene glycolate $[C_2H_4O_2]^{2-}$ and CO dominates when multiple EC molecules are considered (due to intermolecular interactions). The same is observed for the $Ca(ClO_4)_2$ electrolyte. Comparatively, EC initially decomposes on LIB negative electrodes producing lithium ethylene dicarbonate ($LiOCOCH_2CH_2OCOLi$) as main product.[72]

Alternative AIMD simulations of EC, PC, and G4 stabilities against a Ca metal surface indicate that G4 is stable, even at 500 K, while EC and PC receive around 6–25 electrons from the Ca surface.[73] The calculated barriers for cleavage of various

Table 2. Summary of decomposition products formed during electrochemical testing of several Ca electrolyte formulations reported in the literature.

Entry	Electrolyte	Conditions	Products observed at the surface	Techniques used	Refs.
1	Pure THF	Soak a Ca metal electrode for few days	$Ca(OH)_2$	IR	[65]
2	Pure γBL	Soak a Ca metal electrode for few days	Cyclic β-ketoester anion		
3	Pure PC	Soak a Ca metal electrode for few days	$Ca(OH)_2$ and $CaCO_3$		
4	$Ca(ClO_4)_2$ in PC	Soak a Ca metal electrode for few days	$Ca(OH)_2$ and $CaCO_3$		
5	$Ca(ClO_4)_2$ in THF	CV over Ca electrodes	$CaCl_2$, other C and O species		
6	$Ca(AlCl_4)_2$ in $SOCl_2$	Soak a Ca metal electrode for few days	$CaCl_2$	X-ray emission and XRD, SEM	[81]
7	$Ca(BH_4)_2$ in THF	Galvanostatic cycling with a limiting capacity of 1 mAh cm^{-2} at a rate of 1 mA cm^{-2}	Up to 10% CaH_2	Reaction with D_2SO_4 in D_2O + MS of the evolved gases XRD, TOF-SIMS	[83]
8		Galvanostatic deposition at various current densities	Up to 37% CaH_2 at high current density (5 mA cm^{-2})	Reaction with D_2SO_4 in D_2O + MS of the evolved gases XRD, TOF-SIMS	[84]
9	$Ca(BF_4)_2$ in EC:PC	Potentiostatic deposition over Ni or SS substrate at 100 °C	CaF_2, $Ca(OH)_2$, trigonal borate-containing species	IR, XPS, EELS	[85]
10	$Ca[B(hfip)_4]_2$ in G1	Galvanostatic deposition at 0.2 mA cm^{-2} for 20 h	7% CaF_2	EDX, SEM	[87]
11	$Ca[B(hfip)_4]_2$ in G1, THF or G2	Galvanostatic cycling at a rate of 1, 2, 4, and 8 mA cm^{-2}	CaF_2 and "possibly some organic deposits." More CaF_2 when using THF solvent (related with solvation structure)	EDX, SEM	[89]
12	$Ca[CB_{12}H_{12}]_2$ in G1:THF	Galvanostatic cycling	CaH_2, C, O, and B detected by EDX	XRD, EDX	[36]
13	$Ca(TFSI)_2$ in EC:PC	Potentiostatic deposition over Ni or SS substrate at 100 °C	$Ca(OH)_2$, $CaCO_3$, and other amorphous carbon-containing products	IR, XPS, EELS	[85]

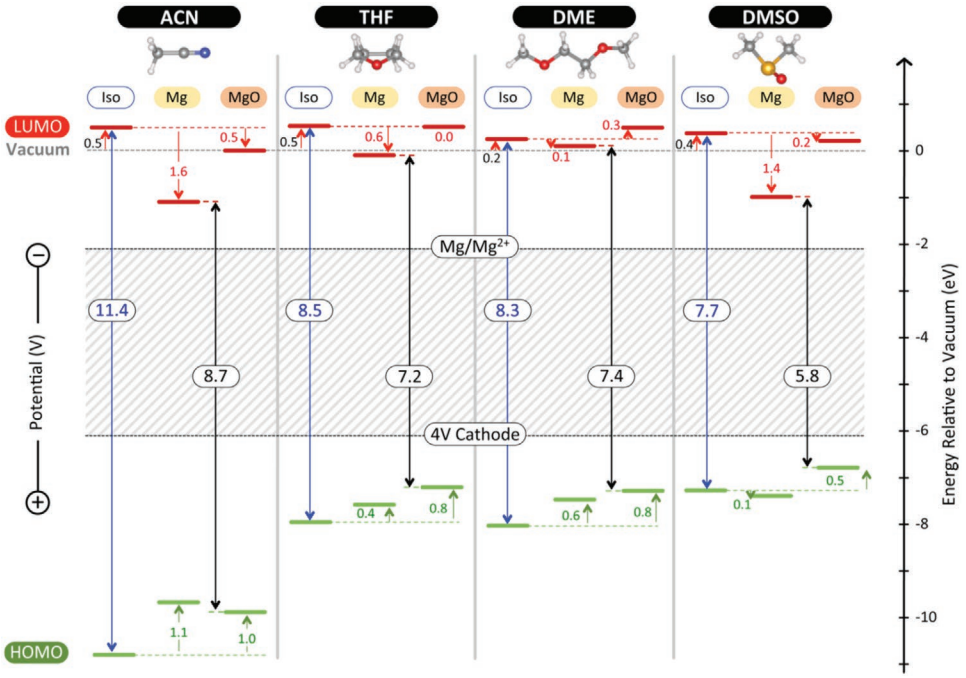

Figure 6. Change in ESW of solvents due to interactions with Mg (0001) and MgO (001) surfaces. The shaded region in the center of the figure represents the electrochemical window of a hypothetical 4 V magnesium battery. DME = G1. Reproduced with permission.[68] Copyright 2016, American Chemical Society.

bonds in EC and PC molecules on the Ca slab are comparable to energy fluctuations at RT (20–70 meV), in agreement with experimental evidence for the decomposition of carbonates in presence of Ca metal. Regarding G4, it may be hypothesized to be stable at the interface with Ca metal, but further studies, including interactions with a Ca salt are needed to verify this assumption.

3.2. Chloride-Containing Electrolytes

As noted above, the development of Mg metal batteries has until very recently focused on organic electrolytes that do not form passivation layers blocking the transport of magnesium.[66] Examples of such are Grignard reagents and chloroaluminate in THF or G1 electrolytes.[74–77]

The presence of Cl^- was shown to have a protective effect, preventing the decomposition of electrolyte components such as PF_6^- and TFSI anions,[78] opening possibilities for development of alternatives to Grignard based electrolytes. Yet the role of Cl^- is not well understood and various hypotheses exist in the literature.

One aspect connects with the possibility to create a functionalized electrode surface. Modeling and operando surface characterization have shown that specific adsorption of chlorides and/or chloride-containing species on the bare magnesium anode are favorable[79] and may inhibit the approach of other anions to the surface. Along the same lines, computational results showed the formation of G1 decomposition products to be unfavorable at the $MgCl_2$ surface,[70] supporting its possible function as Mg surface protective layer in G1-based electrolytes.

Alternatively, the beneficial role of Cl^- could be related to its presence in the complexes formed in mixed $Mg(TFSI)_2$ + $MgCl_2$ based electrolytes (as detailed in Section 2.3). Indeed, $[Mg(G1)_3]^{2+}$ formed in the $Mg(TFSI)_2$ in G1 was found to spontaneously decompose at –0.8 V versus Mg^{2+}/Mg, producing stable $Mg(G1)_2(OCH3)_2$, trapping Mg and preventing its deposition at any reasonable overpotential,[80] which is consistent with the poor Mg plating observed experimentally. If Cl^- is added to the system (i.e., increase in its chemical potential), as in $Mg(TFSI)_2$ + $MgCl_2$ in G1 electrolytes, the presence of the $[Mg(G1)_3]^{2+}$ complex progressively drops and more chlorinated species are formed (**Figure 7**A).[62] At the interface with the Mg electrode, the stability domains of these species are strongly shifted compared to the bulk of the electrolyte because of the strong local electric fields and charges occurring in the double layer, as demonstrated from the Pourbaix diagram at the interface. Remarkably, the $[MgCl_3(G1)]^-$, presumably present only at very high Cl^- chemical potentials (experimentally unattainable), becomes more stable and predominant in the double layer even at much lower Cl^- chemical potentials,[62] before reaching the $MgCl_2$ solubility limit (Figure 7B). By calculating the potential at which electron transfer from the Mg surface to each Mg complex occurs, a kinetic stability limit of –0.3 V versus Mg^{2+}/Mg was deduced for $[Mg_2Cl_2(G1)_4]^{2+}$, while for both $MgCl_2(G1)_2$ and $[MgCl_3(G1)]^-$ electron transfer was not observed down to the computational limit set at –1.6 V versus Mg^{2+}/Mg.

Green zones in Figure 7C show the potential range where Mg^{2+} was found to still thermodynamically reduce to Mg metal (i.e., plating), while the G1 molecules participating in the Mg chlorinated species are not yet electrochemically activated (i.e., no electrolyte decomposition). The potential domain for Mg

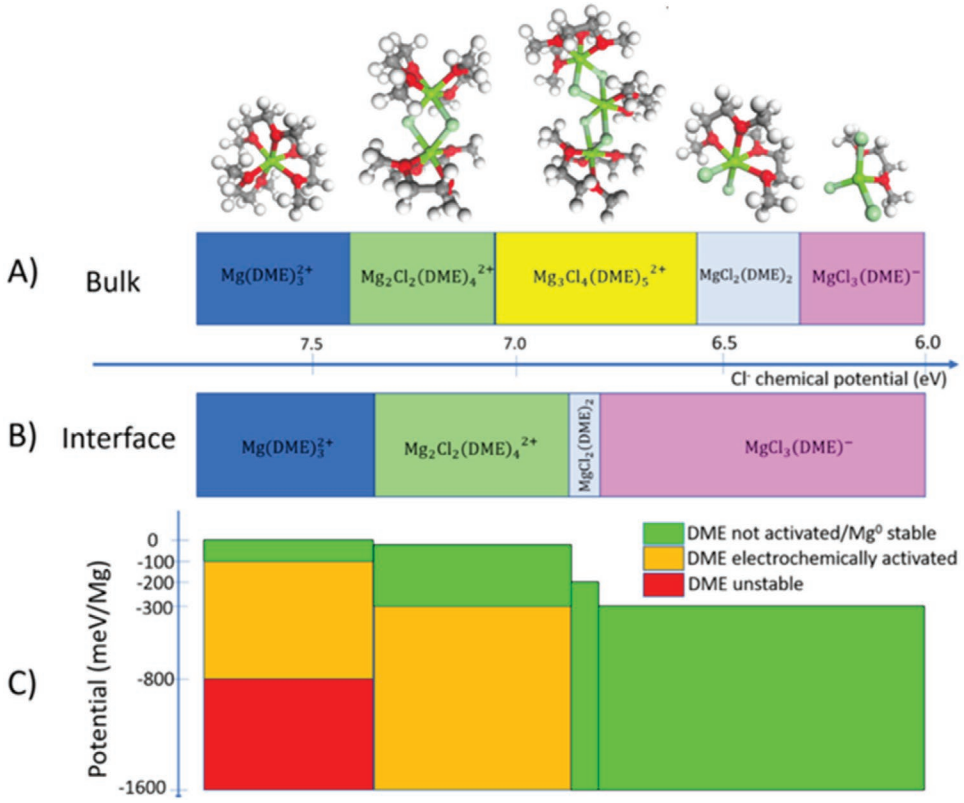

Figure 7. Stable species at the Mg^{2+}/Mg frontier as a function of the chloride chemical potential A) in bulk and B) at the interface. The top panel shows the corresponding DFT optimized structures. C) Stability of Mg-coordinated G1 as a function of the surface species and the applied potential in. Green domains depict the working overpotential, where Mg^{2+} is reduced to Mg but Mg-coordinated G1 remains kinetically stable. Orange zones indicate partial electron transfer to the Mg-coordinated G1, inducing partial activation and increased G1 fragmentation kinetics. In the red zone, the solvate is unstable and spontaneous electrochemical-induced G1 fragmentation occurs. DME = G1. Adapted with permission.[62] Copyright 2021, American Chemical Society.

plating operation domain clearly increases when adding more Cl^-, reaching beyond 1.3 V for $MgCl_2(G1)_2$ and $[MgCl_3(G1)]^-$, which helps explaining the improved stability at the Mg anode induced by the addition of chloride.

Equivalent Grignard electrolytes containing Ca (known as heavy Grignards) have not been used for Ca plating probably due to their difficult preparation processes. The closest related Ca electrolyte containing chloride is $Ca(AlCl_4)_2$ in $SOCl_2$, which decomposes upon contact with a metallic Ca electrode, forming a layer of $CaCl_2$ not enabling the transport of Ca^{2+}.[81] From that point, chloride-based electrolytes have not been further studied.

3.3. Electrolytes with Borohydrides and Other Boron-Containing Anions

The high reductive stability of the BH_4^- anion makes it a suitable option for Mg and Ca electrodeposition from organic electrolytes.

Contrary to $Mg(TFSI)_2$ (Section 3.4), DFT calculations of LUMO levels for solvated $[Mg\text{-}Anion]^+$ ion pairs suggest that $Mg(BH_4)_2$ and $Mg(BF_4)_2$ both are stable against Mg metal reduction.[28] However, explicit interaction with the Mg metal surface, not considered in this study, may influence the LUMO levels of the corresponding species as demonstrated to be the case for several solvents.[68]

This might be the case for $Mg(BH_4)_2$ in G1 electrolytes, in which Arthur et al.[82] detected a boron-containing decomposition product via the B K-edge EXAFS spectra of a platinum WE after 50 cycles of Mg plating/stripping. The clearly observed peak at 190 eV does not correspond to $Mg(BH_4)_2$ nor to a reference B_2O_3 spectrum but seems to be related to hydrogen-based borohydride clusters (B_xH_y).

For $Ca(BH_4)_2$ in THF, CaH_2 was reported as the only byproduct deposited on Au or Pt electrodes when Ca metal is electroplated. The amount of CaH_2 varies between 10 and 37 wt% depending on the current density applied.[83,84] The exact electrolyte decomposition mechanism leading to CaH_2 deposition is still a matter of debate, with some studies suggesting that the anion decomposes producing soluble BH_3 adducts and solid CaH_2,[29] while others propose that dehydrogenation of THF is responsible for the formation of CaH_2.[84]

The passivation layer formed from a $Ca(BF_4)_2$ in EC:PC electrolyte at 100 °C was recently characterized by a combination of XPS, EELS, and IR spectroscopies.[85] Upon polarization, the anion was found to decompose producing a large amount of CaF_2 together with an amorphous boron-containing matrix on

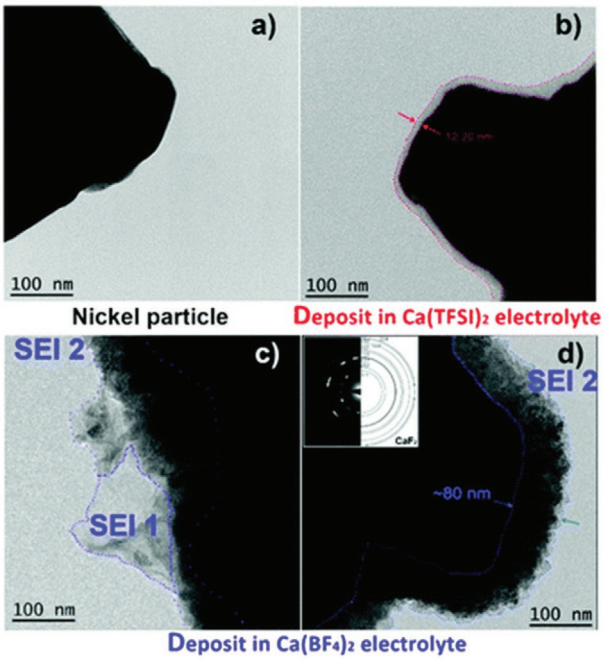

Figure 8. Bright-field TEM images of Ni particles a) before and b,c) and d) after formation of a surface layer in b) $Ca(TFSI)_2$ or c) and d) in $Ca(BF_4)_2$ based electrolytes, respectively. Red and blue dotted lines are as a guide for the eye to indicate the thickness of each passivation layer. The inset in panel (d) corresponds to the diffraction pattern associated to the deposit. Reproduced under the terms of the CC-BY-NC license.[85] Copyright 2020, The Royal Society of Chemistry.

the stainless steel electrode. The EELS and IR spectra suggest that this boron-containing matrix is composed by trigonal (BO_3) moieties, originating from the nucleophilic substitution of F^- ligands of the anion. The resulting surface layer was ≈80 nm thick (**Figure 8**) and IR micro-spectroscopy mapping showed it to be very heterogeneous across the surface.

The surface layers produced from other boron complex anions have been studied by combining XPS, TOF-SIMS, and EDX analysis of working electrode surfaces, and thereby, e.g., Tang et al. showed that $Mg[B(hfip)_4]_2$ in G1 electrolytes are chemically stable in contact with Mg metal at open circuit voltage (OCV). However, when metallic Mg was galvanostatically deposited on a Cu electrode, signals attributed to MgF_2, MgO, and $MgCO_3$ were observed, together with the presence of unidentified boron compounds, pointing toward anion decomposition during plating.[86]

The analogous $Ca[B(hfip)_4]_2$ in G1 electrolyte also showed some degree of anion decomposition, forming different amounts of CaF_2 on the surface depending on the salt concentration.[87,88]

From the studies on $B(hfip)_4$ based electrolytes, only ref. [89] mentions a "possible organic" deposit on the surface of electrodeposited calcium aside from the inorganic CaF_2.

In contrast with the above discussed findings, $Mg(CB_{11}H_{12})_2$ in G4 electrolytes show no decomposition in contact with Mg metal, neither at OCV nor after several galvanostatic plating/stripping cycles.[90,91] Only a very dominant signal of MgO was observed in the Mg 2p XPS spectrum, which is attributed to contamination from the glovebox atmosphere, while the B 1s and C 1s bands are fully explained by residual salt or solvent on the surface, without any new species appearing after cycling (**Figure 9**).

The recent report of Ca reversible plating and stripping using $Ca(CB_{11}H_{12})_2$ in G1 and THF electrolytes mentions the existence of CaH_2 as main side-product (as identified by XRD) on the calcium deposits obtained by galvanostatic deposition over Au electrodes.[36] The differences found between Ca and

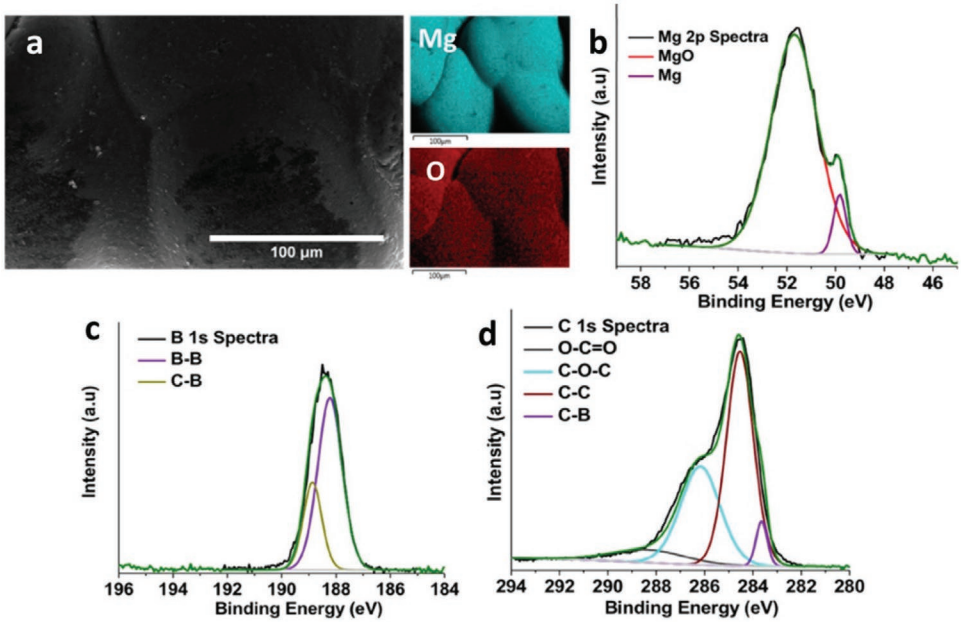

Figure 9. a) SEM image of Mg deposited from the $Mg(CB_{11}H_{12})_2$ electrolyte with EDS elemental mapping; b) Mg 2p, c) B 1s, and d) C 1s XPS spectra of the deposited Mg surface. Reproduced with permission.[91] Copyright 2019, American Chemical Society.

Mg closo-carborane electrolytes are attributed to the lower reduction potential of calcium metal.

Recent DFT and AIMD simulations of the $Ca[B(hfip)_4]_2$ and $Ca(CB_{11}H_{12})_2$ salts stabilities against a Ca metal surface identified $Ca(CB_{11}H_{12})_2$ to be stable, even at 500 K, while one Ca—F bond cleavage was observed for $Ca[B(hfip)_4]_2$.[73] This corroborates experimental evidence for the presence of CaF_2 deposits formed during Ca plating from $Ca[B(hfip)_4]_2$ based electrolytes. Further time-dependent-charge-transfer (TD-CT) calculations between the Ca slab and these salts show transfer of two electrons to $Ca[B(hfip)_4]_2$ and no charge transfer to $Ca(CB_{11}H_{12})_2$. With respect to the apparent discrepancy with the experimental evidence for CaH_2 formation when using $Ca(CB_{11}H_{12})_2$ in G1 or THF electrolytes, we stress again the relevance of considering solvent–salt interactions when performing modeling of the electrolyte stability at a metal electrode. The formation of CaH_2 via a reaction involving also decomposition of THF, as suggested by [83] should also be considered.

3.4. Formulations Containing TFSI

Various studies provide different conclusions regarding the stability of $Mg(TFSI)_2$ based electrolytes with respect to reduction on the surface of magnesium electrodes. After immersing a piece of freshly polished magnesium foil into $Mg(TFSI)_2$ in G3 or G4 electrolytes, a clear signal of MgS and MgF_2 is detected in the XPS spectra of the surfaces, pointing toward anion decomposition.[92] Visual and morphological changes are also observed, together with evident O, F, and S signals in the EDS spectrum of the Mg metal after storage in the $Mg(TFSI)_2$ in G4 electrolyte.[91]

Attempting to rationalize these experimental findings, DFT calculations using an implicit solvation model were performed on both the "free" TFSI anion and a solvated $[Mg\text{-}TFSI]^+$ ion pair.[28] While from the calculated electron affinity (EA) and ionization potential (IP) it was found that the "free" TFSI is stable against reduction and oxidation (up to 2 V vs Mg^{2+}/Mg), it was demonstrated that the cation would reduce if an electron is added to the $[Mg\text{-}TFSI]^+$ ion pair and thus, carrying an unpaired electron, this complex would become chemically active and transient, leading to its rapid decomposition into fragments such as $-CF_3$ and $[CF_3SO_2NSO_2]$-Mg. This evidence for TFSI anion activation upon Mg^{2+} reduction and its subsequent decomposition by cleavage of one of its C—S bonds is consistent with the experimental results cited above.

The formation of monovalent Mg ($Mg^{2+} \rightarrow Mg^+$) in the $[Mg\text{-}TFSI]^0$ reduced ion pair and its reductive stability in G2 was further studied by DFT, explicitly accounting for the interaction with G2.[93] The reductive stability was found to be determined by coordination of the Mg center to the TFSI ion: 1) the complex is stable against decomposition only when two oxygen atoms from TFSI coordinate the Mg center independently of whether 1, 2, or 3 G2 molecules complete the solvation shell; 2) the complex decomposes via TFSI C—S bond cleavage either when coordinated by three oxygen atoms from TFSI and one from G2, or when coordinated by one N atom and one O atom from TFSI and two O atoms from G2. The authors deduce the primary factor determining the stability of the TFSI unit in the $[Mg\text{-}TFSI]^0$ in G2 complex to be the geometry of the complex and stable only when the Mg first solvation shell can accommodate an extra electron on the Mg s-orbital without deforming it.

Experimental evidence for the influence of ion-pair formation on TFSI stability has only been reported rather recently,[94,95] accomplished by combining XPS and operando soft X-ray absorption spectroscopy (SXAS) measurements on $Mg(TFSI)_2$ in different solvents, effectively tailoring the speciation of Mg-TFSI complexes. Decomposition of TFSI was observed when a high proportion of CIPs is present, changing the solvent from 2-MeTHF to a more effective G4 decreased the CIP population and led to less pronounced anion decomposition.

Stability of $Ca(TFSI)_2$ against a Ca metal surface was studied by DFT calculations and AIMD simulations.[73] The AIMD simulations revealed that $Ca(TFSI)_2$ completely decomposes; first, cleavage of the C-S bond occurs, followed by subsequent C—F dissociation within the CF_3 groups, forming various decomposition products, such as CaF_2, CaS, and CaO. This was further corroborated by TD-CT calculations, demonstrating a transfer of eight electrons to occur from the Ca surface to the salt $Ca(TFSI)_2$. Similar results were obtained for the $Ca(PF_6)_2$ salt.

Experimentally, however, the decomposition of a 0.45 M $Ca(TFSI)_2$ in EC:PC electrolyte at 100 °C over a Ca surface produces mainly carbon-containing species (CO_3, C=O, and C—O) and only a modest quantity of CaF_2 (2%).[85] The low extent of TFSI decomposition can be explained by the low concentration of CIPs in this electrolyte; as the Ca^{2+} cations are completely solvated by solvent molecules, only these are carried toward the surface of the electrode and therefore the main building blocks of the formed passivation layer.

3.5. Artificial Surface Coatings for Ca and Mg Electrodes

An artificial Mg^{2+}-conducting interphase based on thermally cyclized polyacrylonitrile was reported by Son et al.[96] to enable reversible Mg plating/stripping in 0.5 M $Mg(TFSI)_2$ in ACN or PC electrolytes. This suggests that the polymeric surface film can sustain the use of reduction-vulnerable electrolytes. Remarkably, this artificial protective layer could sustain more than 40 cycles of a $Mg|V_2O_5$ full cell with an electrolyte containing 3 M of water.

Canepa et al. used DFT calculations to identify possible artificial coatings for Mg anodes with low Mg^{2+} migration barriers and compatibility with Mg metal.[97] The study was limited to binary and ternary inorganic crystalline compounds and found $MgSiN_2$, MgS, MgSe, $MgBr_2$, and MgI_2 as promising candidates for artificial surface coatings.

The stabilization of the Ca metal anode–electrolyte interface by a pre-formed amorphous Al_2O_3 surface coating was recently investigated via a combination of AIMD and standard DFT calculations.[98] It was found that formation of a calcinated phase, $Ca_xAl_2O_3$, is energetically favorable up to $x = 1.5$, and calcination would be accompanied by about 200% volume change. Coating a (001)-terminated metallic Ca with such precalcinated $Ca_{1.5}Al_2O_3$ layer indicates that it may prevent EC decomposition. However, calculations of Ca diffusion coefficients in the $Ca_{0.2}Al_2O_3$ phase at 1400–1600 K yield values of the order 10^{-14} cm^2 s^{-1}, which is 4–6 orders of magnitude lower than typical Li or Na diffusion rates in Al_2O_3, hinting at restricted

Ca^{2+} diffusion even at such elevated temperatures. The same trend is anticipated for higher values of x, but the authors postulate that such diffusion rates may still be sufficiently fast for Ca to diffuse through an Al_2O_3 layer, albeit increased cell impedance.

4. Plating and Stripping Mechanism

Electrodeposition is commonly assumed to occur via the so-called nucleation and growth mechanism where the electrocrystallization takes place after succession of steps: diffusion/migration of the complex cation to the electrode, adsorption with at least partial desolvation, charge transfer, surface diffusion of an adatom, and crystal growth. Each step is associated with an activation energy barrier. In this section, the current knowledge on the parameters affecting Ca and Mg plating kinetics and morphology of the deposit is discussed. For the former, comparisons are made in terms of stripping peak current density in CVs experiments. While not ideal, this allows to consider most of the work published and not to overestimate plating kinetics by considering possible parasitic reduction reactions. If not otherwise specified, the CVs lower cutoff voltage was −1 V versus metal anode pseudo-reference electrode, Pt working electrode, and 25 mV s^{-1} sweep rate were used.

4.1. Chloride-Containing Electrolytes

Anions are usually more weakly solvated than cations due to their smaller charge/radius ratios, resulting in low cation transference numbers, not to be confused with the cation transport number. The latter is defined as the ratio of the electric current derived from a given charged species to the total electric current, while the former gives moles of cations, either "free" or constituent of an ionic species, such as complexes or aggregates, transferred by migration per unit of charge.[99] For infinitely dilute electrolytes, these two quantities could be considered equal, but in the context of battery chemistries based on divalent cation electrolytes, known to exhibit poorer solubility and higher tendency to aggregates and ion pairs formation, the transference number is the more relevant property. Ca and Mg cation transference number (t_+) have been seldom measured in non-aqueous solutions. In 2013, Benmayza et al.[23] calculated the Mg cation complex transference number in DCC solutions to range between 0.018 and 0.19 at 0.40 and 0.15 M, respectively. The decrease of t_+ with increasing electrolyte concentration was attributed to lowered mobility of the dimeric magnesium ions. For the sake of comparison, most of the Li-based electrolytes present cation transference numbers between 0.2 and 0.4.[100] A systematic evaluation of the cation transference number in Mg (and Ca) based electrolytes is still lacking and, considering the extremely low values recorded so far, appears to be critical for the development of new electrolyte formulations.

Even though the transference number of cation complexes tends to decrease with increasing electrolyte concentration, Mg plating and stripping current densities measured during CV increase for most electrolytes until a maximum is reached (**Figure 10**), generally matching the maximum in ionic conductivity of the solution, suggesting a mostly diffusion controlled mass transport of the electro-active species to the electrode. Stripping peak current densities recorded in chloride-containing electrolytes commonly oscillate between 1 and few tens of mA cm^{-2}.

A series of studies relating the Mg^{2+} solvation in chloroaluminate electrolyte with the resulting plating mechanism has been published. As discussed in previous sections, the cationic species present comprise various Mg—Cl complexes expected to play a significant role in the Mg plating process. In ref. [101], a change in the XANES spectra is observed upon polarization of a Pt electrode in an $EtMgCl\text{-}Et_2AlCl$ in THF electrolyte and a monomeric $[MgCl(THF)_5]^+$ complex was proposed as an intermediate adsorbed species before plating. Attias et al.[76] studied the interfacial resistance of a Mg electrode by staircase galvanostatic EIS and measured a high charge-transfer resistance at OCV which quickly diminishes upon polarization (only toward negative potentials). A plating mechanism in which the identity of the adsorbed species changes during the polarization and

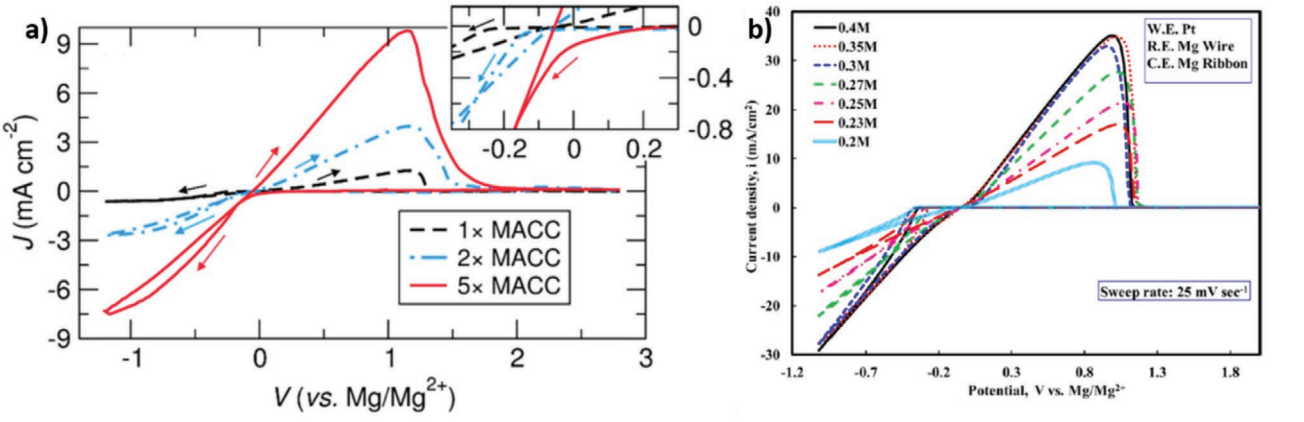

Figure 10. a) Cyclic voltammograms of different DCC electrolyte concentrations in THF (25 mV s^{-1}, $C_2H_5MgCl\text{-}((C_2H_5)_2AlCl)_2$. Adapted with permission.[18] Copyright 2017, American Chemical Society. b) CVs of conditioned MACC electrolytes in THF (5 mV s^{-1}): 60×10^{-3} M $MgCl_2 + 30 \times 10^{-3}$ M $AlCl_3$ (1× MACC), 120×10^{-3} M $MgCl_2 + 60 \times 10^{-3}$ M $AlCl_3$ (2× MACC), and 300 $MgCl_2 + 150 \times 10^{-3}$ M $AlCl_3$ (5× MACC). Reproduced with permission.[23] Copyright 2013, American Chemical Society.

subsequent plating was thus proposed. This would agree with CV measurements using ultramicroelectrodes suggesting the presence of a chemical step prior to electron transfer.[102] Different APC and DCC electrolytes in THF were tested and this initial chemical step was attributed to the disproportionation of the chloro-bridged dimer $[Mg_2(\mu\text{-}Cl)_3(THF)_6]^+$.

The energy required to get rid of all the cation complex ligands (desolvation energy) is another important parameter, especially in divalent cation based systems due to their strong polarizing power. Canepa et al. reported on the adsorption mechanism of $[MgCl(THF)_5]^+$ pointing at the desolvation of the last solvent molecules and the Cl^- ligand as the most energy consuming steps during plating.[103] However, in the absence of passivation layers, the possibility for charge transfer to occur before complete desolvation of the cation complex should also be considered. This would allow to by-pass the high energetic cost for the desolvation of the Cl^- ligand. Charge transfer occurring before complete desolvation would also be in agreement with the measured decrease of the charge transfer resistance (by impedance spectroscopy) when a negative bias potential is applied to a Mg metal anode.[76] If any, the coulombic interaction between Cl^- or solvent ligands with a Mg^0 adatom would be significantly lower than with Mg^+ or Mg^{2+} and would explain why no such charge transfer resistance decrease was measured upon polarization toward positive potentials, because at higher potential the Mg complex remain unchanged.

Connell et al. investigated the role of $MgCl_2$ addition in $Mg(TFSI)_2$ in diglyme electrolytes. By comparison with Zn electrodeposition and the use of different added anions (Cl^-, OTf, TFSI, BF_4^-, PF_6^-) a relationship between stripping polarization and anion association strength was proposed, the addition of Cl^- with a tighter solvation of the Zn cation facilitating stripping.[104] It is however, not obvious that this conclusion can be directly translated to Mg due to the differences in the plating mechanism of the two metals: one versus two step mechanisms respectively for Zn and Mg.[102] The addition of $MgCl_2$ was also found to be effective in preventing Mg metal anode passivation by oxides and hydroxydes and significantly reduced the polarization for Mg stripping even in presence of trace amount of water.[105] The authors demonstrated that, for water content of 0.4×10^{-3} M or lower, passivation layers form only after Mg deposition ceases (in less than a minute, **Figure 11**). These results can explain why most studies on Mg plating do not use Mg metal as working electrode, but mainly Pt instead. This study also highlights the difficulty in fully controlling the experimental conditions and comparing experiments regarding Mg plating, as any differences in terms of water contamination (at the ppm level), OCV period, or time spent at potentials above 0 V versus Mg^{2+}/Mg could affect the reversibility of the plating/stripping process. In this sense, the sweep rate (in mV s^{-1}) and upper potential cutoff are also expected to play an important role in CV experiments as they will determine the amount of time spent above 0 V versus Mg^{2+}/Mg.

4.2. Chloride-Free Electrolytes

Relatively low current densities were recorded in CV experiments using $Mg(BH_4)_2$ based electrolytes. Indeed, at

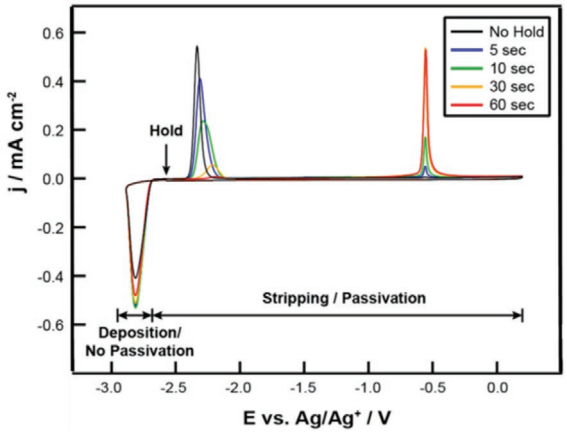

Figure 11. Evolution of electrochemical response (CVs) with varying lengths of potential hold at open circuit after the deposition of a constant amount of Mg, demonstrating the passivation of the electrode surface with the increasing contribution of the Mg stripping peak at –0.5 V versus Ag^+/Ag associated with passivated Mg. Reproduced with permission.[105] Copyright 2016, American Chemical Society.

5 mV s^{-1}, Mg stripping peak current densities lower than 0.05 and 0.3 mA cm^{-2} were measured, respectively, in 0.5 M $Mg(BH_4)_2$ in THF and 0.1 M $Mg(BH_4)_2$ in G1 as electrolytes.[82] These are rather low values as compared with Grignard and other chloride-containing electrolytes (Figure 10). However, adding 0.6 M $LiBH_4$ to 0.18 M $Mg(BH_4)_2$ in G1 resulted in an increase of the Mg stripping peak current density of about two orders of magnitudes (30 mA cm^{-2}) when compared with the one recorded in 0.1 M $Mg(BH_4)_2$ in G1. This study suggests, again, that the coordination shell of the Mg cation (altered by the addition of $LiBH_4$) plays a role in the interfacial processes at the metal surface. While several parameters such as possible formation of Mg-Li alloys, impact of the electrolyte ionic conductivity, and electroactive species mass transport should be further investigated, it is clear that the addition of $LiBH_4$ to the solution has a strong positive impact on the Mg plating/stripping kinetics.

Ca plating using a 1.5 M $Ca(BH_4)_2$ in THF as electrolyte was reported in 2018 by Wang et al. and a stripping peak current density of no less than ≈13 mA cm^{-2} was recorded[83]—hence several orders of magnitude higher than for the Mg systems discussed above, but a systematic comparison is lacking. The plating mechanism using $Ca(BH_4)_2$ in THF as electrolyte was later investigated by Ta et al.[29] and similar current densities were recorded. Using ultramicroelectrodes they reported on a two-step plating mechanism, similar to Mg plating in Grignard based electrolytes, see Section 4.1, involving a chemical step attributed to the dehydrogenation of borohydride catalyzed by the metal substrate. Pt and Au electrodes were then tested, with the latter enabling slightly higher plating /stripping current density, thus stressing the importance of a systematic investigation on the influence of the substrate being used.

Recently, the addition of 0.4 M $LiBH_4$ to a 0.4 M $Ca(BH_4)_2$ in THF electrolyte was also investigated.[54] While longer cyclability of the metal anode was reported, no significant difference was observed in the CVs when adding $LiBH_4$. It is also not clear from this study, how the presence of $LiBH_4$ affect the formation of CaH_2 and thus the nature of the interface.

Using a $Ca[B(hfip)_4]_2$ in G1 electrolyte the current density for Ca stripping ranges between 5 and 30 mAh cm^{-2} depending on the sweep rate, salt concentration, and lower cut-off voltage.[50,87,88] Nielson et al. studied the influence of the solvent on the electrochemical response for $Ca[B(hfip)_4]_2$ electrolytes.[89] Reversible plating and stripping were improved using G2 as solvent as compared to using THF or G1, which resulted both in higher current density/coulombic efficiency and less CaF_2 deposited. This was interpreted from the point-of-view of solvation, with a higher proportion of CIPs in THF and G1. As more anions are bound to Ca^{2+}, they are dragged toward the surface of the electrode upon polarization and are more prone to reduction. In ref. [50], G3 based electrolytes, where no CIPs are present, were reported to not enable reversible electrodeposition. The authors rationalize the result by considering particularly strong interactions for the complexes. Another possibility is that the G3 molecules coordinating the cation are not stable at Ca deposition potentials and, at least partially, passivate the electrode.

In comparison, plating was demonstrated in $Mg[B(hfip)_4]_2$ and $Mg[Al(hfip)_4]_2$ in G1–G4 electrolytes, the current density decreasing with the length of the glyme chain and slightly higher current are recorded using the Al-containing anion.[86]

Recently, the addition of $Mg(BH_4)_2$ to a $Mg[B(hfip)_4]_2$ in G1 electrolyte was found to drastically increase the Mg plating kinetics.[106] While the authors attributed this improvement to the formation of a beneficial passivation layer (mostly composed of MgO, MgF_2, and species that contain −CFx and −COx groups) it is unlikely that such layer would promote Mg^{2+} migration and $Mg(BH_4)_2$ acting as a water scavenger and/or contributing to some extent to favorable modification of the solvation structure is more probable.

Stripping peak current densities of about 6 and 15 mA cm^{-2} (5 mV s^{-1}, lower cutoff voltage: –0.7 V vs Mg^{2+}/Mg) were reported in 0.75 M $Mg(CB_{11}H_{12})_2$, respectively, in G4 and G3.[34] 0.75 M electrolytes prepared by mixing G1 and G2 resulted in an increase in ionic conductivity (≈6 mS cm^{-1}) when compared with G4-based solutions (≈1 mS cm^{-1}) and an increase by about an order of magnitude in terms of the stripping peak current density (100 vs 7 mA cm^{-2}). The latter being among, if not the highest, Mg stripping current density reported up to date.

Finally, to the best of our knowledge, Mg deposition using TFSI based electrolytes with a voltage hysteresis smaller than about 1 V could not be demonstrated without the use of $MgCl_2$ (Section 4.1). With respect to Ca, only prepassivated electrodes with borate-containing interphases allowed for reversible Ca plating and stripping using $Ca(TFSI)_2$ (Section 3.3).[85] In the latter case, a fourfold increase in plating kinetics was recorded during CV experiments when compared with electrolyte containing $Ca(BF_4)_2$ salt, which was ascribed to a lower desolvation energy in TFSI based electrolyte, the latter being mostly CIPs free.

4.3. Deposit Morphology and Dendrite Formation

Aside from the nature of the cation complexes (electro-active species) and presence/composition of interphases, several parameters can affect the plating/stripping processes. Among them, the concentration of electroactive species, the cation transference number, desolvation energy, mobility of adatoms as well as the cell geometry (and current lines) are crucial with respect to plating kinetics and morphology of the deposit.

Smooth plating of a metal is well known to be a complex issue from classical electrochemistry, and mass transport limitation can result in dendritic electrodeposition. Anisotropic metal growth is favored by limited surface diffusion of the adsorbed cations and by an improved hemispherical diffusion at the tip of the dendrite. Until recently, and unlike Li which is known to readily form dendrites at a critical current density >1 mA cm^{-2}, Mg was thought not to be plagued by dendrite formation. Indeed, only a change in the deposit preferred orientation was observed from (0 0 1) to (1 0 0) when increasing current density but dendritic morphology could not be observed up to 2 mA cm^{-2}.[107] The absence, or limited presence, of a passivation layer is a positive feature improving the mass transport toward the electrode. Nondendritic growth of Mg could also be rationalized by theoretical investigations comparing the surface mobility of Li and Mg adatoms pointing at lower self-diffusion barriers of the Mg adatom on (0001), the dominant surface termination upon metal growth.[108] A recent computational study, however, stressed the need for all commonly present facets to be studied.[109] Unfortunately, similar theoretical insights on the mobility of adatoms on Ca metal facets is currently not available.

Few recent studies have evidenced possible formation of Mg and Ca dendrites. Mg dendrites with fractal morphology were observed by Davidson et al.[110] The use of 0.5 M MeMgCl solution in THF and squared shaped electrodes most likely exacerbate poor mass transport and highly inhomogeneous current line distributions and causes dendritic growth. Tests performed in realistic battery conditions are thus required to evaluate exact current density thresholds at which Mg dendrite start to grow.

Using 1 M $Ca(BH_4)_2$ in THF as electrolyte, Pu et al. also demonstrated the formation of Ca dendrites.[84] While a nonoptimal cell configuration was used, with wire type electrodes (**Figure 12**), dendritic growth was only observed at current densities at or above 20 mA cm^{-2}. Again, dendrites tend to form at the sharpest part of the electrode, in this case at the tip of the wires and an estimation of critical current density for dendrite formation in realistic battery conditions is still lacking.

Overall, while it is clear that Ca and Mg dendrites can form in specific conditions, the very complex combination of parameters affecting their growth can explain the difficulty of unambiguously establishing the critical current density at which they start to form. This is a crucial information in order to assess the safety of future Ca and Mg metal batteries. However, the fact that up to 20 mA cm^{-2}, Mg[35] and Ca metal electrodes[84] do not form dendrites is very encouraging. Indeed, Li, which is still considered as a potentially viable metal electrode after several decades of research, is known to readily form dendrites at current density as low as 1 mA cm^{-2}. After only few years of research, Ca and Mg metal anodes can already surpass this current density limitation for dendrite formation by an order of magnitude, placing them as promising candidates for the development of safer batteries.

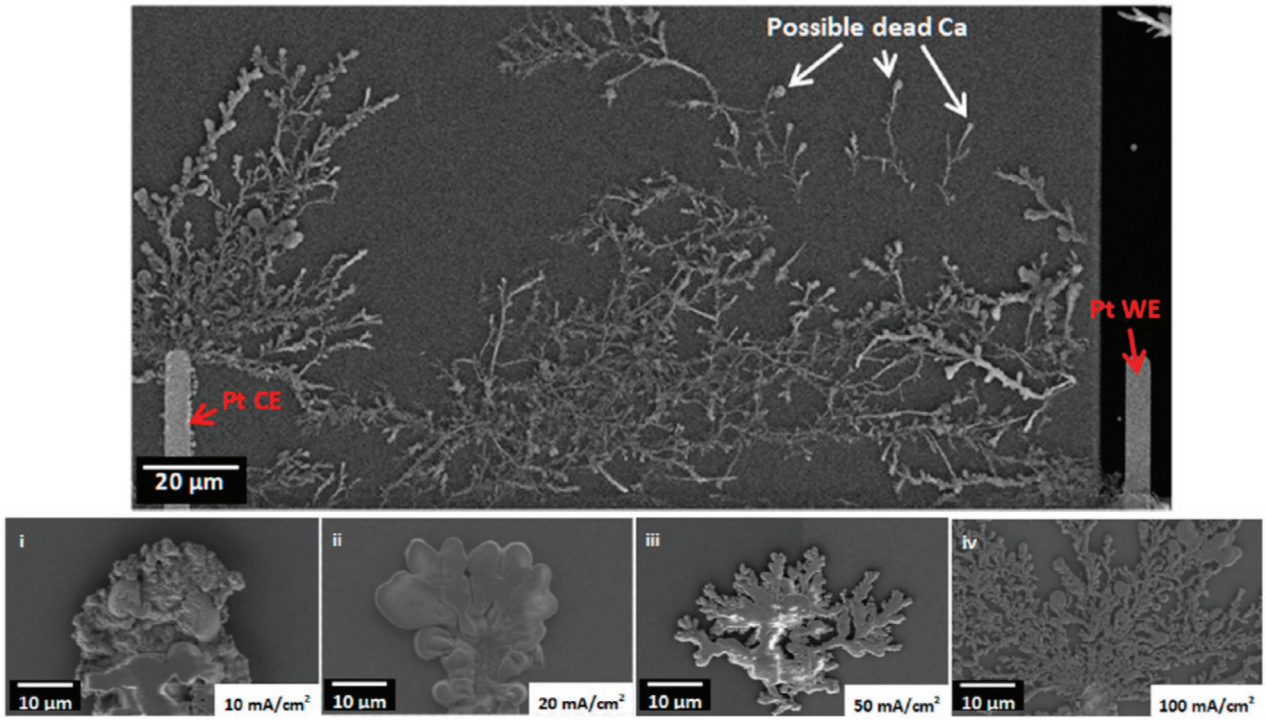

Figure 12. SEM images of Ca deposits under different current densities (electrolyte: 1 M $Ca(BH_4)_2$ in THF). Adapted with permission.[84] Copyright 2020, American Chemical Society.

5. Interfacial Processes and Positive Electrodes

The strong interactions of both divalent cations at hand here with electrolyte solvent molecules and counterions does not only impact on the charge transfer on the negative electrode/electrolyte interface (e.g., for the plating/stripping process), but it also plays a role on the positive electrode side. Inorganic positive electrode materials used in LIBs commonly react through a redox mechanism involving reversible topotactic insertion of ions into a host without any major structural changes. Such materials are required to exhibit a structural framework with interconnected sites wherein the intercalated ion can diffuse and a valence band able to reversibly accept/donate electrons. The rate of ion insertion/deinsertion (ultimately related to the battery power) is often limited by the migration barriers for the guest ions in the host structure, as desolvation of monovalent ions at the interface with the electrolyte is usually not an issue. In contrast, the process of partial desolvation of a divalent cation at the interface with the positive electrode, i.e., its adsorption and loss of remaining ligands before incorporation into the lattice, involves significantly larger energies, especially when CIPs are involved.[47,111]

For instance, DFT calculations of $MgCl^+$ ion pair and $Mg_2Cl_3^+$ dimer desolvation on the most stable (100) surface of the Chevrel phase, Mo_6S_8, indicate that a Mg—Cl bond can be dissociated with a moderate energy cost, as the surface presents Mo undercoordinated metal centers, favoring Cl^- stripping from Mg.[112] In contrast, desolvation of adsorbed $MgCl^+$ and $MgTFSI^+$ ion pairs at the MoO_3 (010) stable surface were found by DFT calculations to be energetically prohibited, although $MgTFSI^+$ dissociation followed by Mg^{2+} insertion may be possible on a hydroxyl-terminated (001) surface.[113] Such results may explain the successful performance of the Chevrel phase as positive electrode, related to its undercoordinated Mo sites, whereas higher-voltage transition metal oxides would only be viable in presence of more weakly coordinating anions. These findings also highlight the role the electrode surface may have on the insertion process, opening possibilities for surface engineering via appropriate synthesis conditions or coatings.

We believe that high desolvation energy barriers are one of the main reason behind the struggle to obtain any performance for several inorganic compounds in multivalent batteries.[4,114] Yet, layered materials with a van der Waals gap that can be expanded in the direction perpendicular to the layers can accommodate larger species such as solvated ions. While partial desolvation may also take place, the composition and structure of these partially-solvated compounds is dependent on the interaction between the solvent dipole and the cations, with kinetics being also impacted by steric factors.[115] This is illustrated by the observed reversible insertion of solvated calcium ions in TiS_2.[116] Although co-insertion results in more severe changes in the structure of the host (larger volume expansion/contraction), this may not be an issue for long term cycling, as deduced from studies dealing with solvated Na insertion in graphite from G2 based electrolytes.[117,118] As the cation first solvation shell is highly dependent on the electrolyte formulation, a solvation shell can, then, be designed so that it best screens the coulombic interactions between the host structure and the divalent ions, enhancing ion migration in the solid. Hence co-insertion could be an approach to follow in the development

of inorganic positive electrode materials. Yet it could involve a penalty in energy density as a larger volume of electrolyte could be needed.

By contrast to insertion type inorganic positive electrodes, it is not clear yet if desolvation is a required step during the redox processes involved when using organic-based positive electrodes. Indeed up to date these compounds demonstrated the highest C rate performances in Mg or Ca cells,[119] possibly due to a combination of parameters including a significantly different mass transport mechanism in the bulk of the electrode and lower (if any) desolvation energy barrier. However, in this case the formation of CIPs is an important parameter to consider as they could lead to a significant decrease in theoretical specific capacity due to the loss of the divalent nature of the charge carrier—hence the possibility to exchange two electrons per redox center.[120]

6. Discussion and Perspectives

Ca and Mg metal batteries have prospects for very high energy densities but, besides finding suitable positive electrodes and compatible electrolytes, the mastering of the plating/stripping processes constitutes an important bottleneck to overcome. This is by no means an easy problem to solve as several interconnected parameters have to be properly understood and subsequently optimized: the cation solvation and desolvation, the nature of the interface between the electrode and the electrolyte (and the potential presence of an interphase), as well as the plating/stripping processes and metal deposit morphology (including avoiding dendrite formation even at high current densities).

Proper understanding of the cation solvation is key to the development of new electrolytes, which has been hampered by several limitations, mostly associated with the divalent nature of the cations. Indeed, the high polarizing power of Mg^{2+} and Ca^{2+} commonly result in the formation of CIPs (especially for Mg) and a low salt solubility. Different strategies have been developed in order to facilitate salt dissociation and/or the formation of non-neutral cation complexes. For instance, the use of solvents with strong chelating properties, such as glymes, or high DNs, such as DMF, instead of high dielectric constant, were both found to improve salt dissociation and prevent the formation of CIPs. Additionally, solvent and/or salt mixing may introduce a competition between ligands, both anions and solvents, in the cation first solvation shell. This strategy shows promise in decreasing cation desolvation energies but needs to be further investigated.

Significant knowledge has been gathered regarding chloride-containing electrolytes as first enablers of Mg electrodeposition. Nonetheless, the role of chloride and how it impacts Mg plating remains a matter of debate. Several reasons have been proposed for the enhanced performance of chloride-containing electrolytes: i) formation of non-neutral monomeric and dimeric complexes affecting the charge transfer process, ii) prevention of ligands decomposition, and iii) functionalization of metal anode surface avoiding passivation and enhancing desolvation. Water contamination and oxide/hydroxide formation on the metal surface (which is produced by ppm-level water impurities) is another major limitation. Chloride-containing electrolytes allow for reversible Mg plating and stripping even in the presence of trace amount of water. However, the use of a noncorrosive water scavenger agent, such as the BH_4^- anion, appears more practical even though alternative anions with higher anodic stabilities are urged for.

As expected from the significant difference between Mg and Ca standard redox potentials, the latter being about 500 mV lower, most studies on Mg metal negative electrodes report mainly the presence of oxides or hydroxides (originating from atmospheric or electrolyte contaminations), whereas, a larger spectrum of different compounds associated to anion or solvent decomposition are found on Ca. However, it is important to highlight that the stability of electrolyte components is also strongly affected by their interactions with the cation. For instance, decomposition of the TFSI anion is observed in Mg-based electrolytes, as it is more prone to CIP formation, while it was reported to be stable in Ca cells.

Unlike Mg, reversible Ca plating/stripping was demonstrated in presence of interphases, CaH_2 or borate based. While in its infancy, the development of artificial cation conductive interphases has been proposed for Mg and holds promise for improved practical handling of the metal, by limiting the reactivity with trace amounts of water in the electrolyte or humidity during cell assembly. Interphases at the metal negative electrodes would also allow greater flexibility in terms of electrolyte choices as components unstable against the metal itself could possibly be used. Caution should, however, be exercised when designing such interphases as they ideally should enable complete desolvation of the cation—and this might possibly have a prohibitive energy barrier, especially if CIPs are formed, leading to low power performance at the cell level.

Systematic fundamental insights on the plating/stripping mechanisms are also largely lacking. For instance, it is expected that the cation transference number in the electrolyte can play an important role in plating kinetics, but it is seldom measured. While extremely low t_+ (<0.1) are expected in the divalent cation based electrolytes developed so far, detailed studies on the controlling parameters are much needed. At present, the cation mass transport is expected to take place mostly through diffusion—hence the importance put on the ionic conductivity. This can, at least partially, explain the significant improvement in plating kinetics observed in mixed salt formulations as the added salt can act as a supporting electrolyte favoring diffusion. Additional research efforts are required in order to evaluate/tune the cation complex mass transport mechanism.

With respect to the metal deposit morphology and dendrite formation, it comes to no surprise that Ca and Mg dendrites may form under specific cycling conditions. Indeed, dendrite formation is inherent to any electrodeposition process and occurs if mass transport is the limiting step and will hence form over a certain current density threshold, which also is strongly dependent on the cell geometry. However, the studies reported so far do not unambiguously clarify the current density threshold, much as the cell designs used are far from realistic for practical battery application. Thus systematic studies using "real" battery operating conditions are needed to ascertain if Ca and Mg metal negative electrodes are viable and safe options. Nonetheless, preliminary results obtained with both $Ca(BH_4)_2$

in THF and $Mg(CB_{11}H_{12})_2$ in a mixture of glymes electrolytes, respectively, are both very encouraging, as there is no dendrite formation at or below 20 mA cm^{-2}.

On the positive electrode side, desolvation energy at the interface with the electrolyte will play a major role in the reversibility of insertion/de-insertion and power performance at the cell level. Therefore, strategies such as engineering of the cation solvation and/or the electrode surface, via functionalization or coating, should be explored. Considering the very strong columbic interactions with solvents and/or anions, alternative positive electrodes should also be investigated. Electrodes allowing for co-insertion of cation ligands, similar to the Na-diglyme complex in graphite, possibly lowering the desolvation energy barrier, are potential candidates. We also believe that the development of organic positive electrodes is currently the most promising avenue for "high power" Ca and Mg battery cells.

Overall, systematic studies are largely lacking, especially for Ca metal batteries for which a very narrow spectrum of electrolytes enabling plating/stripping have been reported. Historically, most studies deal with only one aspect of these systems; either solvation, passivation layer formation or plating mechanism/dendrite formation, with little attention given to the overall picture. As more experimental techniques become available, recent studies attempt to correlate between many or all of these different phenomena.

A similar picture is obtained for computational studies and their linkages to experimental results. Ab initio and DFT methods are commonly used for calculating bulk properties of battery materials, both electrodes and electrolytes, in general, but there is a lack of systematic investigations. The situation with respect to modeling of battery interfaces is more critical, as reliable modeling concepts and tools are less developed. At present, studies of interfaces and interfacial processes in multivalent batteries are mainly based on calculations of the electrolyte ESW via HOMO/LUMO analysis or species adsorption and dissociation energies at surfaces, and only recently a few more complete formalisms have been developed. One aspect specific to batteries based on liquid electrolytes that further complicates computational studies of the interface is the possibility for the electrolyte to decompose and form intermediate products, which greatly impacts on the electrochemical reactions to be considered. Hence, extensive computational insight on these very complex systems is needed, and foreseen to play a major role in designing better electrolytes and interfaces as well as better understanding plating mechanisms.

Acknowledgements

J.D.F.-S. and D.S.T. contributed equally to this work. Funding from the European Union's Horizon 2020 research and innovation programme ERC-2016-STG (CAMBAT Grant Agreement No. 715087) and H2020 FETOPEN-1-2016-2017 (CARBAT, Grant Agreement No. 766617) is gratefully acknowledged. ICMAB-CSIC members thank the Spanish Agencia Estatal de Investigación Severo Ochoa Programme for Centres of Excellence in R&D (CEX2019-000917-S). J.D.F.-S. is grateful to 2020-MSCA-COFUND-2016 (DOC-FAM, Grant Agreement No. 754397). J.D.F.-S. contributed to this work in the frame of the Doctoral Degree Program in Materials Science by the Universitat Autònoma de Barcelona.

Conflict of Interest

The authors declare no conflict of interest.

Keywords

calcium and magnesium batteries, interface, plating, SEI, solvation

Received: August 22, 2021
Revised: October 13, 2021
Published online:

[1] A. Ponrouch, J. Bitenc, R. Dominko, N. Lindahl, P. Johansson, M. R. Palacin, *Energy Storage Mater.* **2019**, *20*, 253.
[2] D. Aurbach, Z. Lu, A. Schechter, Y. Gofer, H. Gizbar, R. Turgeman, Y. Cohen, M. Moshkovich, E. Levi, *Nature* **2000**, *407*, 724.
[3] D. Monti, A. Ponrouch, R. B. Araujo, F. Barde, P. Johansson, M. R. Palacín, *Front. Chem.* **2019**, *7*, 79.
[4] M. E. Arroyo-de Dompablo, A. Ponrouch, P. Johansson, M. R. Palacín, *Chem. Rev.* **2020**, *120*, 6331.
[5] A. M. Melemed, A. Khurram, B. M. Gallant, *Batteries Supercaps* **2020**, *3*, 570.
[6] R. Dominko, J. Bitenc, R. Berthelot, M. Gauthier, G. Pagot, V. Di Noto, *J. Power Sources* **2020**, *478*, 229027.
[7] J. Muldoon, C. B. Bucur, T. Gregory, *Chem. Rev.* **2014**, *114*, 11683.
[8] H. Gizbar, Y. Vestfrid, O. Chusid, Y. Gofer, H. E. Gottlieb, V. Marks, D. Aurbach, *Organometallics* **2004**, *23*, 3826.
[9] Y. Vestfried, O. Chusid, Y. Goffer, P. Aped, D. Aurbach, *Organometallics* **2007**, *26*, 3130.
[10] L. F. Wan, D. Prendergast, *J. Am. Chem. Soc.* **2014**, *136*, 14456.
[11] Y. Nakayama, Y. Kudo, H. Oki, K. Yamamoto, Y. Kitajima, K. Noda, *J. Electrochem. Soc.* **2008**, *155*, A754.
[12] N. Pour, Y. Gofer, D. T. Major, D. Aurbach, *J. Am. Chem. Soc.* **2011**, *133*, 6270.
[13] D. Aurbach, I. Weissman, Y. Gofer, E. Levi, *Chem. Rec.* **2003**, *3*, 61.
[14] H. S. Kim, T. S. Arthur, G. D. Allred, J. Zajicek, J. G. Newman, A. E. Rodnyansky, A. G. Oliver, W. C. Boggess, J. Muldoon, *Nat. Commun.* **2011**, *2*, 427.
[15] Y. Guo, F. Zhang, J. Yang, F. Wang, Y. NuLi, S. Hirano, *Energy Environ. Sci.* **2012**, *5*, 9100.
[16] R. E. Doe, R. Han, J. Hwang, A. J. Gmitter, I. Shterenberg, H. D. Yoo, N. Pour, D. Aurbach, *Chem. Commun.* **2014**, *50*, 243.
[17] K. A. See, K. W. Chapman, L. Zhu, K. M. Wiaderek, O. J. Borkiewicz, C. J. Barile, P. J. Chupas, A. A. Gewirth, *J. Am. Chem. Soc.* **2016**, *138*, 328.
[18] K. A. See, Y.-M. Liu, Y. Ha, C. J. Barile, A. A. Gewirth, *ACS Appl. Mater. Interfaces* **2017**, *9*, 35729.
[19] T. Liu, J. T. Cox, D. Hu, X. Deng, J. Hu, M. Y. Hu, J. Xiao, Y. Shao, K. Tang, J. Liu, *Chem. Commun.* **2015**, *51*, 2312.
[20] O. Mizrahi, N. Amir, E. Pollak, O. Chusid, V. Marks, H. Gottlieb, L. Larush, E. Zinigrad, D. Aurbach, *J. Electrochem. Soc.* **2008**, *155*, A103.
[21] G. Bieker, M. Salama, M. Kolek, Y. Gofer, P. Bieker, D. Aurbach, M. Winter, *ACS Appl. Mater. Interfaces* **2019**, *11*, 24057.
[22] P. Canepa, S. Jayaraman, L. Cheng, N. N. Rajput, W. D. Richards, G. S. Gautam, L. A. Curtiss, K. A. Persson, G. Ceder, *Energy Environ. Sci.* **2015**, *8*, 3718.
[23] A. Benmayza, M. Ramanathan, T. S. Arthur, M. Matsui, F. Mizuno, J. Guo, P.-A. Glans, J. Prakash, *J. Phys. Chem. C* **2013**, *117*, 26881.
[24] Y. Li, S. Guan, H. Huo, Y. Ma, Y. Gao, P. Zuo, G. Yin, *Adv. Funct. Mater.* **2021**, *31*, 2100650.
[25] H.-W. Li, Y. Yan, S. Orimo, A. Züttel, C. M. Jensen, *Energies* **2011**, *4*, 185.

[26] N. T. Hahn, J. Self, K. S. Han, V. Murugesan, K. T. Mueller, K. A. Persson, K. R. Zavadil, *J. Phys. Chem. B* **2021**, *125*, 3644.
[27] R. Mohtadi, M. Matsui, T. S. Arthur, S.-J. Hwang, *Angew. Chem., Int. Ed.* **2012**, *51*, 9780.
[28] N. N. Rajput, X. Qu, N. Sa, A. K. Burrell, K. A. Persson, *J. Am. Chem. Soc.* **2015**, *137*, 3411.
[29] K. Ta, R. Zhang, M. Shin, R. T. Rooney, E. K. Neumann, A. A. Gewirth, *ACS Appl. Mater. Interfaces* **2019**, *11*, 21536.
[30] N. T. Hahn, J. Self, T. J. Seguin, D. M. Driscoll, M. A. Rodriguez, M. Balasubramanian, K. A. Persson, K. R. Zavadil, *J. Mater. Chem. A* **2020**, *8*, 7235.
[31] D. R. MacFarlane, M. Forsyth, E. I. Izgorodina, A. P. Abbott, G. Annat, K. Fraser, *Phys. Chem. Chem. Phys.* **2009**, *11*, 4962.
[32] R. B. Araujo, V. Thangavel, P. Johansson, *Energy Storage Mater.* **2021**, *39*, 89.
[33] S. H. Strauss, *Chem. Rev.* **1993**, *93*, 927.
[34] O. Tutusaus, R. Mohtadi, T. S. Arthur, F. Mizuno, E. G. Nelson, Y. V. Sevryugina, *Angew. Chem., Int. Ed.* **2015**, *54*, 7900.
[35] H. Dong, O. Tutusaus, Y. Liang, Y. Zhang, Z. Lebens-Higgins, W. Yang, R. Mohtadi, Y. Yao, *Nat. Energy* **2020**, *5*, 1043.
[36] K. Kisu, S. Kim, T. Shinohara, K. Zhao, A. Züttel, S. Orimo, *Sci. Rep.* **2021**, *11*, 7563.
[37] D. M. Driscoll, N. K. Dandu, N. T. Hahn, T. J. Seguin, K. A. Persson, K. R. Zavadil, L. A. Curtiss, M. Balasubramanian, *J. Electrochem. Soc.* **2020**, *167*, 160512.
[38] T. Mandai, Y. Youn, Y. Tateyama, *Mater. Adv.* **2021**, *2*, 6283.
[39] Y. M. Lee, J. E. Seo, N.-S. Choi, J.-K. Park, *Electrochim. Acta* **2005**, *50*, 2843.
[40] M. Shakourian-Fard, G. Kamath, S. M. Taimoory, J. F. Trant, *J. Phys. Chem. C* **2019**, *123*, 15885.
[41] W. A. Henderson, *Electrolytes for Lithium and Lithium-ion Batteries*, Springer, New York **2014**, pp. 1–92.
[42] S. Terada, T. Mandai, S. Suzuki, S. Tsuzuki, K. Watanabe, Y. Kamei, K. Ueno, K. Dokko, M. Watanabe, *J. Phys. Chem. C* **2016**, *120*, 1353.
[43] T. Kimura, K. Fujii, Y. Sato, M. Morita, N. Yoshimoto, *J. Phys. Chem. C* **2015**, *119*, 18911.
[44] N. Sa, N. N. Rajput, H. Wang, B. Key, M. Ferrandon, V. Srinivasan, K. A. Persson, A. K. Burrell, J. T. Vaughey, *RSC Adv.* **2016**, *6*, 113663.
[45] M. Salama, I. Shterenberg, H. Gizbar, N. N. Eliaz, M. Kosa, K. Keinan-Adamsky, M. Afri, L. J. W. Shimon, H. E. Gottlieb, D. T. Major, Y. Gofer, D. Aurbach, *J. Phys. Chem. C* **2016**, *120*, 19586.
[46] M. Hattori, K. Yamamoto, M. Matsui, K. Nakanishi, T. Mandai, A. Choudhary, Y. Tateyama, K. Sodeyama, T. Uchiyama, Y. Orikasa, Y. Tamenori, T. Takeguchi, K. Kanamura, Y. Uchimoto, *J. Phys. Chem. C* **2018**, *122*, 25204.
[47] J. D. Forero-Saboya, E. Marchante, R. B. Araujo, D. Monti, P. Johansson, A. Ponrouch, *J. Phys. Chem. C* **2019**, *123*, 29524.
[48] K. Fujii, M. Sogawa, N. Yoshimoto, M. Morita, *J. Phys. Chem. B* **2018**, *122*, 8712.
[49] P. Kubisiak, A. Eilmes, *J. Phys. Chem. C* **2018**, *122*, 12615.
[50] N. T. Hahn, D. M. Driscoll, Z. Yu, G. E. Sterbinsky, L. Cheng, M. Balasubramanian, K. R. Zavadil, *ACS Appl. Energy Mater.* **2020**, *3*, 8437.
[51] F. Tuerxun, Y. Abulizi, Y. NuLi, S. Su, J. Yang, J. Wang, *J. Power Sources* **2015**, *276*, 255.
[52] Y. Shao, T. Liu, G. Li, M. Gu, Z. Nie, M. Engelhard, J. Xiao, D. Lv, C. Wang, J.-G. Zhang, J. Liu, *Sci. Rep.* **2013**, *3*, 3130.
[53] J. Chang, R. T. Haasch, J. Kim, T. Spila, P. V. Braun, A. A. Gewirth, R. G. Nuzzo, *ACS Appl. Mater. Interfaces* **2015**, *7*, 2494.
[54] Y. Jie, Y. Tan, L. Li, Y. Han, S. Xu, Z. Zhao, R. Cao, X. Ren, F. Huang, Z. Lei, G. Tao, G. Zhang, S. Jiao, *Angew. Chem., Int. Ed.* **2020**, *59*, 12689.
[55] H. Wang, X. Feng, Y. Chen, Y. S. Liu, K. S. Han, M. Zhou, M. H. Engelhard, V. Murugesan, R. S. Assary, T. L. Liu, W. Henderson, Z. Nie, M. Gu, J. Xiao, C. Wang, K. Persson, D. Mei, J. G. Zhang, K. T. Mueller, J. Guo, K. Zavadil, Y. Shao, J. Liu, *ACS Energy Lett.* **2020**, *5*, 200.
[56] J. Z. Hu, N. N. Rajput, C. Wan, Y. Shao, X. Deng, N. R. Jaegers, M. Hu, Y. Chen, Y. Shin, J. Monk, Z. Chen, Z. Qin, K. T. Mueller, J. Liu, K. A. Persson, *Nano Energy* **2018**, *46*, 436.
[57] Z. Ma, M. Kar, C. Xiao, M. Forsyth, D. R. MacFarlane, *Electrochem. Commun.* **2017**, *78*, 29.
[58] K. Shimokawa, H. Matsumoto, T. Ichitsubo, *J. Phys. Chem. Lett.* **2018**, *9*, 4732.
[59] I. Shterenberg, M. Salama, H. D. Yoo, Y. Gofer, J.-B. Park, Y.-K. Sun, D. Aurbach, *J. Electrochem. Soc.* **2015**, *162*, A7118.
[60] D.-T. Nguyen, A. Y. S. Eng, M.-F. Ng, V. Kumar, Z. Sofer, A. D. Handoko, G. S. Subramanian, Z. W. Seh, *Cell Rep. Phys. Sci.* **2020**, *1*, 100265.
[61] N. Sa, B. Pan, A. Saha-Shah, A. A. Hubaud, J. T. Vaughey, L. A. Baker, C. Liao, A. K. Burrell, *ACS Appl. Mater. Interfaces* **2016**, *8*, 16002.
[62] A. K. Lautar, J. Bitenc, R. Dominko, J.-S. Filhol, *ACS Appl. Mater. Interfaces* **2021**, *13*, 8263.
[63] M. Salama, I. Shterenberg, L. J. W. Shimon, K. Keinan-Adamsky, M. Afri, Y. Gofer, D. Aurbach, *J. Phys. Chem. C* **2017**, *121*, 24909.
[64] Y. Gofer, R. Turgeman, H. Cohen, D. Aurbach, *Langmuir* **2003**, *19*, 2344.
[65] D. Aurbach, R. Skaletsky, Y. Gofer, *J. Electrochem. Soc.* **1991**, *138*, 3536.
[66] Z. Lu, A. Schechter, M. Moshkovich, D. Aurbach, *J. Electroanal. Chem.* **1999**, *466*, 203.
[67] Y. Yu, A. Baskin, C. Valero-Vidal, N. T. Hahn, Q. Liu, K. R. Zavadil, B. W. Eichhorn, D. Prendergast, E. J. Crumlin, *Chem. Mater.* **2017**, *29*, 8504.
[68] N. Kumar, D. J. Siegel, *J. Phys. Chem. Lett.* **2016**, *7*, 874.
[69] T. T. Tran, W. M. Lamanna, M. N. Obrovac, *J. Electrochem. Soc.* **2012**, *159*, A2005.
[70] J. S. Lowe, D. J. Siegel, *J. Phys. Chem. C* **2018**, *122*, 10714.
[71] J. Young, M. Smeu, *J. Phys. Chem. Lett.* **2018**, *9*, 3295.
[72] S. K. Heiskanen, J. Kim, B. L. Lucht, *Joule* **2019**, *3*, 2322.
[73] S. S. R. K. C. Yamijala, H. Kwon, J. Guo, B. M. Wong, *ACS Appl. Mater. Interfaces* **2021**, *13*, 13114.
[74] D. Aurbach, A. Schechter, M. Moshkovich, Y. Cohen, *J. Electrochem. Soc.* **2001**, *148*, A1004.
[75] D. Aurbach, Y. Gofer, A. Schechter, O. Chusid, H. Gizbar, Y. Cohen, M. Moshkovich, R. Turgeman, *J. Power Sources* **2001**, *97*, 269.
[76] R. Attias, B. Dlugatch, M. S. Chae, Y. Goffer, D. Aurbach, *Electrochem. Commun.* **2021**, *124*, 106952.
[77] J. Muldoon, C. B. Bucur, A. G. Oliver, T. Sugimoto, M. Matsui, H. S. Kim, G. D. Allred, J. Zajicek, Y. Kotani, *Energy Environ. Sci.* **2012**, *5*, 5941.
[78] I. Shterenberg, M. Salama, Y. Gofer, D. Aurbach, *Langmuir* **2017**, *33*, 9472.
[79] R. Attias, M. Salama, B. Hirsch, Y. Goffer, D. Aurbach, *Joule* **2019**, *3*, 27.
[80] A. K. Lautar, J. Bitenc, T. Rejec, R. Dominko, J.-S. Filhol, M.-L. Doublet, *J. Am. Chem. Soc.* **2020**, *142*, 5146.
[81] R. J. Staniewicz, *J. Electrochem. Soc.* **1980**, *127*, 782.
[82] T. S. Arthur, P.-A. Glans, N. Singh, O. Tutusaus, K. Nie, Y.-S. Liu, F. Mizuno, J. Guo, D. H. Alsem, N. J. Salmon, R. Mohtadi, *Chem. Mater.* **2017**, *29*, 7183.
[83] D. Wang, X. Gao, Y. Chen, L. Jin, C. Kuss, P. G. Bruce, *Nat. Mater.* **2018**, *17*, 16.
[84] S. D. Pu, C. Gong, X. Gao, Z. Ning, S. Yang, J.-J. Marie, B. Liu, R. A. House, G. O. Hartley, J. Luo, P. G. Bruce, A. W. Robertson, *ACS Energy Lett.* **2020**, *5*, 2283.
[85] J. Forero-Saboya, C. Davoisne, R. Dedryvère, I. Yousef, P. Canepa, A. Ponrouch, *Energy Environ. Sci.* **2020**, *13*, 3423.

[86] K. Tang, A. Du, S. Dong, Z. Cui, X. Liu, C. Lu, J. Zhao, X. Zhou, G. Cui, *Adv. Mater.* **2020**, *32*, 1904987.
[87] Z. Li, O. Fuhr, M. Fichtner, Z. Zhao-Karger, *Energy Environ. Sci.* **2019**, *12*, 3496.
[88] A. Shyamsunder, L. E. Blanc, A. Assoud, L. F. Nazar, *ACS Energy Lett.* **2019**, *4*, 2271.
[89] K. V. Nielson, J. Luo, T. L. Liu, *Batteries Supercaps* **2020**, *3*, 766.
[90] N. T. Hahn, T. J. Seguin, K.-C. Lau, C. Liao, B. J. Ingram, K. A. Persson, K. R. Zavadil, *J. Am. Chem. Soc.* **2018**, *140*, 11076.
[91] R. Jay, A. W. Tomich, J. Zhang, Y. Zhao, A. De Gorostiza, V. Lavallo, J. Guo, *ACS Appl. Mater. Interfaces* **2019**, *11*, 11414.
[92] H. Kuwata, M. Matsui, N. Imanishi, *J. Electrochem. Soc.* **2017**, *164*, A3229.
[93] A. Baskin, D. Prendergast, *J. Phys. Chem. C* **2016**, *120*, 3583.
[94] F. Tuerxun, K. Yamamoto, M. Hattori, T. Mandai, K. Nakanishi, A. Choudhary, Y. Tateyama, K. Sodeyama, A. Nakao, T. Uchiyama, M. Matsui, K. Tsuruta, Y. Tamenori, K. Kanamura, Y. Uchimoto, *ACS Appl. Mater. Interfaces* **2020**, *12*, 25775.
[95] F. Tuerxun, K. Yamamoto, T. Mandai, Y. Tateyama, K. Nakanishi, T. Uchiyama, T. Watanabe, Y. Tamenori, K. Kanamura, Y. Uchimoto, *J. Phys. Chem. C* **2020**, *124*, 28510.
[96] S. B. Son, T. Gao, S. P. Harvey, K. X. Steirer, A. Stokes, A. Norman, C. Wang, A. Cresce, K. Xu, C. Ban, *Nat. Chem.* **2018**, *10*, 532.
[97] T. Chen, G. Sai Gautam, P. Canepa, *Chem. Mater.* **2019**, *31*, 8087.
[98] J. Young, M. Smeu, *Adv. Theory Simul.* **2021**, *4*, 2100018.
[99] P. G. Bruce, *Solid State Electrochemistry*, Cambridge University Press, Cambridge **1997**.
[100] K. Xu, *Chem. Rev.* **2004**, *104*, 4303.
[101] F. Mizuno, N. Singh, T. S. Arthur, P. T. Fanson, M. Ramanathan, A. Benmayza, J. Prakash, Y. S. Liu, P. A. Glans, J. Guo, *Front. Energy Res.* **2014**, *2*, 46.
[102] K. Ta, K. A. See, A. A. Gewirth, *J. Phys. Chem. C* **2018**, *122*, 13790.
[103] P. Canepa, G. S. Gautam, R. Malik, S. Jayaraman, Z. Rong, K. R. Zavadil, K. Persson, G. Ceder, *Chem. Mater.* **2015**, *27*, 3317.
[104] J. G. Connell, M. Zorko, G. Agarwal, M. Yang, C. Liao, R. S. Assary, D. Strmcnik, N. M. Markovic, *ACS Appl. Mater. Interfaces* **2020**, *12*, 36137.
[105] J. G. Connell, B. Genorio, P. P. Lopes, D. Strmcnik, V. R. Stamenkovic, N. M. Markovic, *Chem. Mater.* **2016**, *28*, 8268.
[106] Z. Li, T. Diemant, Z. Meng, Y. Xiu, A. Reupert, L. Wang, M. Fichtner, Z. Zhao-Karger, *ACS Appl. Mater. Interfaces* **2021**, *13*, 33123.
[107] M. Matsui, *J. Power Sources* **2011**, *196*, 7048.
[108] M. Jäckle, K. Helmbrecht, M. Smits, D. Stottmeister, A. Groß, *Energy Environ. Sci.* **2018**, *11*, 3400.
[109] A. K. Lautar, D. Kopač, T. Rejec, T. Bančič, R. Dominko, *Phys. Chem. Chem. Phys.* **2019**, *21*, 2434.
[110] R. Davidson, A. Verma, D. Santos, F. Hao, C. Fincher, S. Xiang, J. Van Buskirk, K. Xie, M. Pharr, P. P. Mukherjee, S. Banerjee, *ACS Energy Lett.* **2019**, *4*, 375.
[111] M. Okoshi, Y. Yamada, A. Yamada, H. Nakai, *J. Electrochem. Soc.* **2013**, *160*, A2160.
[112] L. F. Wan, B. R. Perdue, C. A. Apblett, D. Prendergast, *Chem. Mater.* **2015**, *27*, 5932.
[113] L. F. Wan, D. Prendergast, *J. Phys. Chem. C* **2018**, *122*, 398.
[114] P. Canepa, G. Sai Gautam, D. C. Hannah, R. Malik, M. Liu, K. G. Gallagher, K. A. Persson, G. Ceder, *Chem. Rev.* **2017**, *117*, 4287.
[115] R. Schöllhorn, *Intercalation Chemistry*, Elsevier, Amsterdam **1982**, pp. 315–360.
[116] D. S. Tchitchekova, A. Ponrouch, R. Verrelli, T. Broux, C. Frontera, A. Sorrentino, F. Bardé, N. Biskup, M. E. Arroyo-de Dompablo, M. R. Palacín, *Chem. Mater.* **2018**, *30*, 847.
[117] B. Jache, P. Adelhelm, *Angew. Chem., Int. Ed.* **2014**, *53*, 10169.
[118] H. Kim, J. Hong, Y.-U. Park, J. Kim, I. Hwang, K. Kang, *Adv. Funct. Mater.* **2015**, *25*, 534.
[119] P. Poizot, J. Gaubicher, S. Renault, L. Dubois, Y. Liang, Y. Yao, *Chem. Rev.* **2020**, *120*, 6490.
[120] J. Bitenc, A. Scafuri, K. Pirnat, M. Lozinšek, I. Jerman, J. Grdadolnik, B. Fraisse, R. Berthelot, L. Stievano, R. Dominko, *Batteries Supercaps* **2021**, *4*, 214.
[121] Z. Song, Z. Zhang, A. Du, S. Dong, G. Li, G. Cui, *J. Energy Chem.* **2020**, *48*, 299.
[122] O. Tutusaus, R. Mohtadi, N. Singh, T. S. Arthur, F. Mizuno, *ACS Energy Lett.* **2017**, *2*, 224.
[123] C. J. Barile, E. C. Barile, K. R. Zavadil, R. G. Nuzzo, A. A. Gewirth, *J. Phys. Chem. C* **2014**, *118*, 27623.
[124] J. H. Connor, W. E. Reid, G. B. Wood, *J. Electrochem. Soc.* **1957**, *104*, 38.
[125] S.-J. Kang, H. Kim, S. Hwang, M. Jo, M. Jang, C. Park, S.-T. Hong, H. Lee, *ACS Appl. Mater. Interfaces* **2019**, *11*, 517.
[126] Y. Zhou, M. Su, X. Yu, Y. Zhang, J.-G. Wang, X. Ren, R. Cao, W. Xu, D. R. Baer, Y. Du, O. Borodin, Y. Wang, X.-L. Wang, K. Xu, Z. Xu, C. Wang, Z. Zhu, *Nat. Nanotechnol.* **2020**, *15*, 224.

Juan D. Forero-Saboya is currently undergoing his doctoral studies in Materials Science at the Universitat Autònoma de Barcelona, after completing his master's in materials for Energy Storage and Conversion (MESC). He works at the Solid State Chemistry Department at the Institut de Ciencia de Materials (ICMAB-CSIC, Spain) developing electrolyte formulations for divalent metal batteries. His research focuses on the solvation properties of cations in battery electrolytes, novel electrolyte formulations, and general development of next-generation battery concepts.

Deyana S. Tchitchekova received her Ph.D. in Chemistry from University of Sherbrooke (Canada) in 2011, for the modeling of molecules driven by intense ultrashort laser fields. After postdoctoral works at University College London (UK) involving simulations of laser–molecule interactions, and at Institut de Radioprotection et Sûreté Nucléaire (France) related to the ageing of nuclear vessel steels, she joined the Solid State Chemistry Department at the Institut de Ciencia de Materials (ICMAB-CSIC, Spain), where she works as postdoctoral researcher on multivalent battery chemistries.

Patrik Johansson is Full Professor in Physics at Chalmers University of Technology, Sweden, as well as being co-director of ALISTORE-ERI, one of Europe's largest industry-academia networks within the field of modern batteries, and vice-director of the Graphene Flagship, one of Europe's largest joint research efforts all categories. He received his Ph.D. in Inorganic Chemistry in 1998 from Uppsala University, Sweden and has continuously aimed at combining understanding of new materials at the molecular scale, often via ab initio/DFT computational methods and IR/Raman spectroscopy, with battery concept development and real battery performance—with a special interest in all kinds of electrolytes.

M. Rosa Palacin, after a Ph.D. in solid state chemistry (UAB, 1995) and a postdoctoral stay at LRCS (Amiens, France), she joined the Institut de Ciencia de Materials de Barcelona (ICMAB-CSIC, Spain) where she is currently a research professor, being also actively involved in ALISTORE-ERI. Her scientific career has been fully focused in rechargeable battery materials with specific emphasis set in the study of electrode materials. She worked on nickel-based and lithium-based technologies to more recently deviate to alternative chemistries such as sodium-ion and multivalent systems.

Alexandre Ponrouch received his Ph.D. in 2010 from the Institut National de la Recherche Scientifique (INRS-EMT, Canada) working on electrodeposition of metals, alloys, and oxides nanotubes and nanowires for application in fuel cells and supercapacitors. He is currently staff researcher at Institut de Ciència de Materials de Barcelona (ICMAB-CSIC, Spain). His research is mainly focused on fundamental electrochemistry applied to the development of new electrolytes, interfaces, and interphases for post Li batteries, including Na-ion, Ca, and Mg.